International Journal of Non-Linear Mechanics 74 (2015) 108–121

Contents lists available at ScienceDirect

International Journal of Non-Linear Mechanics

journal homepage: www.elsevier.com/locate/nlm

# Modelling the curing process in magneto-sensitive polymers: Rate-dependence and shrinkage

Mokarram Hossain [a], Prashant Saxena [a,b], Paul Steinmann [a,*]

[a] Chair of Applied Mechanics, University of Erlangen-Nuremberg, Egerlandstr. 5, 91058 Erlangen, Germany
[b] Center for Integrative Genomics, Génopode Building, University of Lausanne, 1015 Lausanne, Switzerland

ARTICLE INFO

*Article history:*
Received 6 February 2015
Received in revised form
12 April 2015
Accepted 14 April 2015
Available online 22 April 2015

*Keywords:*
Magneto-sensitive polymers
Polymer curing
Magneto-mechanical coupled problem
Magneto-viscoelasticity
Curing shrinkage

ABSTRACT

This paper deals with a phenomenologically motivated magneto-viscoelastic coupled finite strain framework for simulating the curing process of polymers under the application of a coupled magneto-mechanical load. Magneto-sensitive polymers are prepared by mixing micron-sized ferromagnetic particles in uncured polymers. Application of a magnetic field during the curing process causes the particles to align and form chain-like structures lending an overall anisotropy to the material. The polymer curing is a viscoelastic complex process where a transformation from fluid to solid occurs in the course of time. During curing, volume shrinkage also occurs due to the packing of polymer chains by chemical reactions. Such reactions impart a continuous change of magneto-mechanical properties that can be modelled by an appropriate constitutive relation where the temporal evolution of material parameters is considered. To model the shrinkage during curing, a magnetic-induction-dependent approach is proposed which is based on a multiplicative decomposition of the deformation gradient into a mechanical and a magnetic-induction-dependent volume shrinkage part. The proposed model obeys the relevant laws of thermodynamics. Numerical examples, based on a generalised Mooney–Rivlin energy function, are presented to demonstrate the model capacity in the case of a magneto-viscoelastically coupled load.



## 1. Introduction and outline

In the last decades several classes of smart materials have been invented and the so-called magnetorheological elastomers (MREs) or magneto-active elastomers are a relatively new group of smart materials that have obtained considerable attention. The mechanical properties such as the shear modulus of MREs can be enhanced by the application of a magnetic field. MREs are prepared using magnetically permeable, mainly iron particles which are embedded in a non-magnetically active polymeric matrix. One of the reasons for mechanical property enhancements in the entire MREs system is due to mutual interactions between particles and between the particles and the bulk matrix. An external magnetic load to MREs results in significant changes in their macroscopic properties, i.e. such excitation can vary the material stiffness and damping properties that make MREs attractive candidates for various technical applications. Applications include different components in automotive industry, civil engineering devices, e.g. suspension bushing, brakes, smart springs in dynamic vibration absorber, building vibration isolation, noise barrier system and sensors [2,13,15,20].

The application of an external magnetic field as well as the dispersion of iron particles in the polymeric matrix can be achieved in two ways [14,16,18]. Firstly, when the bulk polymer matrix is exposed to a magnetic field during curing, the ferromagnetic particles are magnetised and form chain-like structures in the direction of the applied magnetic field. This results in anisotropic elastomers where the magnetic particles are aligned in a particular orientation. Such particularly oriented magnetorheological elastomers show anisotropy in mechanical, magnetic and thermal properties [10]. Secondly, if there is no application of the magnetic load during the entire curing process, especially just after start of the curing process, the iron particles will have a random isotropic distribution in the composite [12,14]. Microstructures of these composites are typically studied using imaging techniques such as scanning electron microscopy (SEM) or computerised tomography (CT). When a magnetic field is applied to fully cured MREs, the iron-particles apply magnetic forces on each other thereby causing an overall deformation of the polymeric matrix as well as generation of internal stresses. This phenomenon is observed macroscopically as magnetostriction or change of stiffness.

* Corresponding author. Tel.: +49 9131 8528501; fax: +49 9131 8528503.
*E-mail addresses:* mokarram.hossain@ltm.uni-erlangen.de (M. Hossain), prashant.saxena@unil.ch (P. Saxena), paul.steinmann@ltm.uni-erlangen.de (P. Steinmann).

http://dx.doi.org/10.1016/j.ijnonlinmec.2015.04.008
0020-7462/

During the curing process of polymers, a series of chemical reactions occur which transforms a viscoelastic fluid into a viscoelastic solid. Due to successive reactions, polymer chains cross-link to each other. Hence, the formation of new chemical bonds allows the chains to come closer. Such packing of chains results in a decrease in the specific volume which is observed as the volume or curing shrinkage. In order to capture all relevant phenomena during curing, Lion and co-workers [29,32] proposed a phenomenologically inspired thermo-viscoelastic curing model for finite strains which includes thermally and chemically induced volume changes via a ternary multiplicative decomposition of the deformation gradient into mechanical, thermal and chemical parts. The model is extended by Liebl et al. [27,28] to incorporate plasticity-like deformation effects with a yield stress depending on the temperature and degree of cure, as well as isotropic hardening. Similar ideas are incorporated to develop continuum-based models in the case of chemical ageing of polymers, cf. [30,31]. For further review on the constitutive modelling of the purely mechanical curing process of polymers, we refer to the papers by Hossain et al. [21–24] and Klinge et al. [34].

Several papers [10,13,14] reported experimental works both on isotropic and anisotropic magneto-sensitive polymeric composites. Moreover, a considerable amount of literature can be found mainly discussing modelling and simulation of isotropic and anisotropic magneto-active elastomers in the framework of large deformation, cf. Bustamante et al. [3–5], Dorfmann and Ogden [7,8], and Brigadnov and Dorfmann [6]. However, there is no constitutive model, to the best of the authors' knowledge, that can predict material parameter evolution as well as stiffness gain during the curing process in the presence of a magnetic field or a magnetic induction. During the preparation of particle-filled MREs, residual stresses might generate due to an uneven or differential curing (well-known as a warpage phenomenon) of the composites, particularly if the thickness of a sample becomes large. Moreover, if the mould is constrained to disallow movements in some directions, there will be shrinkage-generated stresses that can eventually debond composites from the mould. Therefore, modelling and simulation tools can be optimal ways to predict and minimise these pathological phenomena. Since the elastomeric matrix can undergo large deformations when excited by an external magnetic induction, a finite strain framework is essential to predict the curing process behaviour under the application of a magneto-mechanically coupled load. The proposed modelling framework is within the hypoelastic concept of our previously published purely mechanical curing model [21–23]. To extend the approach for a magneto-mechanically coupled load, a phenomenologically motivated convolution integral type energy potential is proposed that consists of three parts, i.e. a pure mechanical part, a pure magnetic part and a magneto-mechanically coupled part [43]. The energy potential is formulated considering some physical observations that are reported to happen during curing processes, cf. Kiasat [33] and Gillen [35]. One of the important physical phenomena is that a curing material does not change its stress state as resulted from previous deformations – even though its material properties continue to evolve until it changes the current state of deformation. This observation is extended for the magnetic loading also, see Hossain et al. [43]. Another assumption is considered herein which was adapted earlier for a purely mechanical curing model development that during the curing process all relevant material parameters are simultaneously experiencing temporal evolutions. The above two approaches are not restricted to elasticity but can also be used for viscoelastic material models, as will be discussed in this paper.

The paper is organised as follows: Section 2 will briefly review a compressible magneto-viscoelastic model for fully cured elastomers. This constitutive relation is a modified form of our recently proposed magneto-mechanical model for fully cured MREs [38]. In Section 3, the main mathematical foundation that leads to a constitutive relation for the polymer curing process in the presence of a magneto-mechanically coupled load is discussed in detail. A viscoelastic extension of the elastic framework developed in Section 3 is shown in Section 4. A novel approach to model the curing-induced volume shrinkage is proposed that is based on a multiplicative decomposition of the deformation gradient into mechanical and magnetic induction-produced shrinkage parts in Section 5 while the evolution of various time-dependent material parameters appearing in the free energy function is discussed in Section 6. To perform numerical computations based on the framework developed in Section 4, a Mooney–Rivlin based magneto-mechanical free energy function is chosen and necessary derivations are given. The final Section 7 presents some numerical examples which illustrate that the proposed model can capture relevant phenomena of polymer curing in the presence of a magneto-mechanically coupled field.

## 2. Viscoelasticity in magneto-sensitive polymers

In the following section we briefly review the magneto-viscoelastic model [38,39] that has been extended in this paper to incorporate curing. The classical approach in viscoelastic rubber-like material modelling is the multiplicative decomposition of the deformation gradient into elastic and viscous (inelastic) parts as

$$\boldsymbol{F} = \boldsymbol{F}_e \boldsymbol{F}_v, \tag{1}$$

which yields further relations, e.g. $\boldsymbol{C}_e = \boldsymbol{F}_e^t \boldsymbol{F}_e$ and $\boldsymbol{C}_v = \boldsymbol{F}_v^t \boldsymbol{F}_v$, cf. Lubliner [36], Reese and Govindjee [37] and the references cited therein for detailed discussions of the kinematic quantities. The second order tensor $\boldsymbol{C}_v$ is the three-dimensional equivalent of the viscous deformation of a dashpot in a standard rheological element [37]. The response of MREs to a magnetic field is usually time-dependent and hence results in dissipation. In order to account for these effects, the magnetic kinematic variable $\mathbb{B}$ is decomposed into an equilibrium and a non-equilibrium component as was originally proposed in [38],

$$\mathbb{B} = \mathbb{B}_e + \mathbb{B}_v. \tag{2}$$

For the case of MREs, the alignment and reorientation of magnetic filler particles due to the applied magnetic field can be relatively slow. Hence, a dissipative component $\mathbb{B}_v$ of the magnetic field is a meaningful concept in the case of long characteristic times. Following the analogy of a multiplicative decomposition of the deformation gradient and an additive decomposition of the magnetic induction vector, the total magneto-mechanical energy stored in a body can be decomposed into an equilibrium part and a non-equilibrium part, cf. Lubliner [36] and Reese and Govindjee [37],

$$\Omega(\boldsymbol{a}, \boldsymbol{C}, \boldsymbol{C}_v, \mathbb{B}, \mathbb{B}_v) = \Omega_{eq}(\boldsymbol{a}, \boldsymbol{C}, \mathbb{B}) + \Omega_{neq}(\boldsymbol{a}, \boldsymbol{C}, \boldsymbol{C}_v, \mathbb{B}, \mathbb{B}_v), \tag{3}$$

where $\boldsymbol{a}$ is the unit vector in the direction of anisotropy.

During the curing of an MRE, the direction of anisotropy generated in the composite is the same as the direction of applied magnetic induction. This, along with the arguments of material frame indifference, leads to a simplification (see, for example, Appendix A and Ref. [43]), wherein the energy density function is dependent on only six scalar invariants

$$I_1 = \boldsymbol{C} : \boldsymbol{I}, \quad I_2 = \tfrac{1}{2}\left[I_1^2 - \boldsymbol{C}^2 : \boldsymbol{I}\right], \quad I_3 = \sqrt{\det \boldsymbol{C}},$$
$$I_4 = [\mathbb{B} \otimes \mathbb{B}] : \boldsymbol{I}, \quad I_5 = [[\boldsymbol{C}\mathbb{B}] \otimes \mathbb{B}] : \boldsymbol{I}, \quad I_6 = [[\boldsymbol{C}\mathbb{B}] \otimes [\boldsymbol{C}\mathbb{B}]] : \boldsymbol{I}, \tag{4}$$

$\boldsymbol{I}$ being the second order identity tensor in the material configuration.

As a first example to model magneto-viscoelasticity for a fully cured particle-filled elastomer, the equilibrium part of the energy density function is considered to be a generalisation of the classical Mooney–Rivlin function with compressible terms to

magnetoelasticity of the form

$$\Omega_{eq}=\frac{\mu}{4}\left[1+\alpha_e\tanh\left(\frac{I_4}{m_e}\right)\right]\left[[1+\chi][I_1-3]+[1-\chi][I_2-3]\right]+qI_4+rI_6+\frac{1}{8}\kappa[\ln I_3]^2-\frac{1}{2}\mu\ln I_3. \tag{5}$$

In Eq. (5) $\mu,\kappa,q,r$ are material parameters while $\alpha_e,m_e,\chi$ are scaling constants. The factor $[1+\alpha_e\tanh(I_4/m_e)]$ with a non-dimensionalisation parameter $m_e$ and a dimensionless positive parameter $\alpha_e$ for scaling is included in the energy function to incorporate an increase in the stiffness due to magnetisation. The parameters $q$ and $r$ can be termed as the magnetoelastic coupling parameters which have the dimensions of $\mu_0^{-1}$, where $\mu_0$ is the magnetic permeability of vacuum. If we put $\alpha_e=q=r=0$, Eq. (5) simplifies to the classical Mooney–Rivlin elastic energy density function widely used to model elastomers, cf. [25,26]. The non-equilibrium part of the energy density function is considered to be a generalisation of the classical Neo-Hooke function to magnetoelasticity of the form

$$\Omega_{neq}(\boldsymbol{C},\boldsymbol{C}_v,\mathbb{B},\mathbb{B}_v)=\frac{\mu_v}{2}\left[\boldsymbol{C}_v^{-1}:\boldsymbol{C}-3\right]+q_v[[\mathbb{B}-\mathbb{B}_v]\otimes[\mathbb{B}-\mathbb{B}_v]]:\boldsymbol{I}+r_v[[\boldsymbol{C}[\mathbb{B}-\mathbb{B}_v]]\otimes[\boldsymbol{C}[\mathbb{B}-\mathbb{B}_v]]]:\boldsymbol{I}+\frac{1}{2}\kappa_v[\ln J_e]^2-\mu_v\ln J_e \tag{6}$$

where $\mu_v,\kappa_v,q_v,r_v$ are viscous material parameters and $J_e=\det\boldsymbol{F}_e$. A thermodynamically consistent evolution of the viscous magnetic variable $\mathbb{B}_v$ is

$$\frac{d\mathbb{B}_v}{dt}=\frac{2\mu_0}{T_m}\left[q_v\boldsymbol{I}+r_v\boldsymbol{C}^2\right][\mathbb{B}-\mathbb{B}_v]. \tag{7}$$

To track the evolution of the mechanical strain-like internal variable $\boldsymbol{C}_v$, we use a linear finite strain type evolution equation [37]

$$\frac{d\boldsymbol{C}_v}{dt}=\frac{1}{T_v}[\boldsymbol{C}-\boldsymbol{C}_v]. \tag{8}$$

In the equations above, $T_v$ is considered to be the relaxation time that accounts for the relaxation phenomenon in the viscoelastic component while $T_m$ is the same for its magnetic counterpart.

## 3. Curing in magneto-elasticity

During the curing process continuous chain cross-linking occurs due to chemical reactions. Such chemical cross-linking yields increasing stiffness of a material under curing which can be conceptualised as the addition of more and more elastic elements to the already formed network. Addition of more spring-like elements will result in an increment of the material stiffness. An important physical observation [33,35] during curing is that even though the material's properties are changing continuously, the material will not change its stress state unless its state of deformation is changed. Since we do not have additional experimental data that illustrates the evolution of magnetic parameters during curing as well as the stiffness gain under a magneto-mechanically load, we follow the same above-stated observation that is considered in the mechanical deformation to the case of the magnetic induction. This assumption motivates us to take a magneto-elastically coupled energy potential in the form of a convolution integral under the presence of a magneto-mechanically coupled load as

$$\Phi(t)=\frac{1}{2}\int_0^t\left[\mathcal{A}'(\tau):[\boldsymbol{E}(t)-\boldsymbol{E}(\tau)]\right]:[\boldsymbol{E}(t)-\boldsymbol{E}(\tau)]\,d\tau+\frac{1}{2}\int_0^t\left[\mathcal{K}'(\tau)\cdot[\mathbb{B}(t)-\mathbb{B}(\tau)]\right]\cdot[\mathbb{B}(t)-\mathbb{B}(\tau)]\,d\tau+\int_0^t\left[\mathcal{C}'(\tau)\cdot[\mathbb{B}(t)-\mathbb{B}(\tau)]\right]:[\boldsymbol{E}(t)-\boldsymbol{E}(\tau)]\,d\tau. \tag{9}$$

In Eq. (9) $\mathcal{A}'(\tau)=d\mathcal{A}(\tau)/d\tau$, $\mathcal{K}'(\tau)=d\mathcal{K}(\tau)/d\tau$ and $\mathcal{C}'(\tau)=d\mathcal{C}(\tau)/d\tau$, where $\boldsymbol{E}$ is the Green–Lagrange strain tensor and $\mathbb{B}$ is the magnetic induction vector in the material configuration. The free energy density $\Phi$ defined in Eq. (9) can be interpreted as the total, accumulated energy density of an evolving system while the strain energy density $\Omega$ (decomposed into $\Omega_{\text{eq}}$ and $\Omega_{\text{neq}}$ for viscoelastic cases) is rather related to the body response to the current state of deformations. The latter energy density is required to define the three time-dependent fourth order, third order and second order magnetoelastic moduli tensors, i.e. $\mathcal{A},\mathcal{C},\mathcal{K}$, respectively. Now we need a magneto-elastic coupled free energy function that is frequently used for fully cured magneto-sensitive elastomers to derive the relations for these time-dependent stiffness moduli, i.e.

$$\mathcal{A}(t)=\frac{\partial^2\Omega(t)}{\partial\boldsymbol{E}\partial\boldsymbol{E}},\quad \mathcal{C}(t)=\frac{\partial^2\Omega(t)}{\partial\boldsymbol{E}\partial\mathbb{B}},\quad \mathcal{K}(t)=\frac{\partial^2\Omega(t)}{\partial\mathbb{B}\partial\mathbb{B}}, \tag{10}$$

where $\Omega(t)$ is a coupled energy function for magneto-elastic polymers with time dependent material parameters [11]. In order to establish a thermodynamically consistent constitutive relation for the curing process, the model has to fulfill the second law of thermodynamics in the form of the Clausius–Duhem inequality which, for the isothermal process, can be written in the case of a magneto-elastic coupled problem as

$$\boldsymbol{S}:\dot{\boldsymbol{E}}+\mathbb{H}\cdot\dot{\mathbb{B}}-\dot{\Phi}\geq 0, \tag{11}$$

where $\boldsymbol{S}$, $\mathbb{H}$ and $\Phi$ are the second Piola–Kirchhoff stress tensor, the magnetic field vector in the material configuration and the potential function proposed in Eq. (9), respectively. Using the standard Coleman–Noll procedure with the help of the Leibnitz integral rule the evolution of the stress and the magnetic field follows in rate forms as

$$\dot{\boldsymbol{S}}(t)=\tfrac{1}{2}\mathcal{A}(t):\dot{\boldsymbol{C}}(t)+\mathcal{C}(t)\cdot\dot{\mathbb{B}}(t), \tag{12}$$

$$\dot{\mathbb{H}}(t)=\tfrac{1}{2}\mathcal{C}^t(t):\dot{\boldsymbol{C}}(t)+\mathcal{K}(t)\cdot\dot{\mathbb{B}}(t), \tag{13}$$

where $\mathcal{C}^t=\partial^2\Omega/\partial\mathbb{B}\partial\boldsymbol{E}$. The mathematical derivation leading to Eqs. (12) and (13) is detailed in [43] and therefore omitted here. Note that our previously proposed finite strain constitutive framework for a purely mechanical curing is based on a hypoelastic type, i.e. rate-form relation for stress–strain. We apply the same analogy for the magneto-mechanical curing relation. Therefore, the resulting equations (12) for the stress development and (13) for the magnetic field development during curing are hypoelastic type relations. These relations capture the physical observation that a curing material subjected to no change of current loading (mechanical and magnetic) will not change its response (mechanical and magnetic) as resulted from previous loading – even though its material properties are continuously evolving. Discretising Eqs. (12) and (13) with an Euler-backward type implicit integrator, we obtain

$$\boldsymbol{S}^{n+1}=\boldsymbol{S}^n+\tfrac{1}{2}\mathcal{A}^{n+1}:[\boldsymbol{C}^{n+1}-\boldsymbol{C}^n]+\mathcal{C}^{n+1}\cdot[\mathbb{B}^{n+1}-\mathbb{B}^n], \tag{14}$$

and

$$\mathbb{H}^{n+1}=\mathbb{H}^n+\tfrac{1}{2}\mathcal{C}^{t,n+1}:[\boldsymbol{C}^{n+1}-\boldsymbol{C}^n]+\mathcal{K}^{n+1}\cdot[\mathbb{B}^{n+1}-\mathbb{B}^n], \tag{15}$$

where $[\bullet]^n=[\bullet](t_n)$, $t_{n+1}=t_n+\Delta t$ and $\Delta t$ is a time step.

## 4. Curing in magneto-viscoelasticity

The additive decomposition of the total stress into a time-independent equilibrium part and a time-dependent non-equilibrium part is a classical approach in finite strain viscoelasticity. We proposed a similar approach [38] for the fully cured magneto-viscoelastic polymers, i.e.

$$\boldsymbol{S}^{n+1}=\boldsymbol{S}_{eq}^{n+1}+\boldsymbol{S}_{neq}^{n+1}, \tag{16}$$

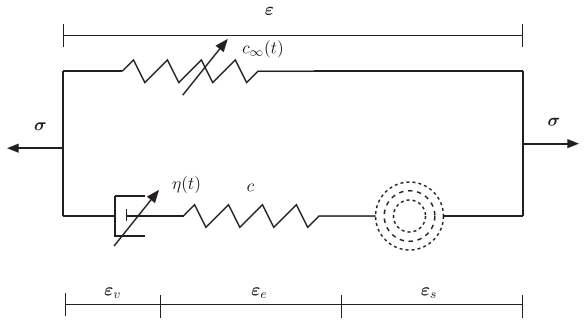


**Fig. 1.** One-dimensional cure-dependent mechanical viscoelastic model with a shrinkage element of deformation $\varepsilon_s$. It mimics the idea of a Zener-type viscoelastic standard solid model with a time-dependent spring, a time-dependent dash-pot and a time-dependent shrinkage-induced fictitious element connected in parallel.

and

$$\mathbb{H}^{n+1} = \mathbb{H}_{eq}^{n+1} + \mathbb{H}_{neq}^{n+1}. \tag{17}$$

To extend the cure-dependent magneto-elastic constitutive framework developed in Section 3, we utilise the idea of a fully cured magneto-viscoelastic modelling as in Saxena et al. [38] and the idea of a purely mechanical viscoelastic cure-dependent model as in Hossain et al. [22]. Thus, we add the non-equilibrium responses (stress and magnetic field) with the magneto-elastic curing formulations developed in Section 3. This, in the case of pure mechanical curing, can be idealised as a finite strain formulation of a rheologically motivated standard solid model in linear cure-dependent viscoelasticity, cf. Fig. 1. Note that in the case of cure-dependent magneto-viscoelasticity, different to classical viscoelasticity, both contributions (equilibrium and non-equilibrium) depend on time now, not only the non-equilibrium part. The equilibrium part $\boldsymbol{S}_{eq}$ of Eq. (16) is just replaced by the thermodynamically consistent magneto-mechanical cure-dependent relation in Eq. (14), i.e.

$$\begin{aligned}\boldsymbol{S}^{n+1} &= \boldsymbol{S}_{eq}^{n+1} + \boldsymbol{S}_{neq}^{n+1}\\ \boldsymbol{S}^{n+1} &= \underbrace{\boldsymbol{S}_{eq}^{n} + \tfrac{1}{2}\mathcal{A}^{n+1} : [\boldsymbol{C}^{n+1} - \boldsymbol{C}^{n}] + \mathcal{C}^{n+1} \cdot [\mathbb{B}^{n+1} - \mathbb{B}^{n}]}_{\boldsymbol{S}_{eq}^{n+1}} + \boldsymbol{S}_{neq}^{n+1}.\end{aligned} \tag{18}$$

A similar analogy is applied for the magnetic field–magnetic induction relationship, i.e. the equilibrium part $\mathbb{H}_{eq}^{n+1}$ of Eq. (17) is replaced by the thermodynamically consistent magneto-mechanical cure-dependent relation in Eq. (15), i.e.

$$\begin{aligned}\mathbb{H}^{n+1} &= \mathbb{H}_{eq}^{n+1} + \mathbb{H}_{neq}^{n+1}\\ \mathbb{H}^{n+1} &= \underbrace{\mathbb{H}_{eq}^{n} + \tfrac{1}{2}\mathcal{C}^{t,n+1} : [\boldsymbol{C}^{n+1} - \boldsymbol{C}^{n}] + \mathcal{K}^{n+1} \cdot [\mathbb{B}^{n+1} - \mathbb{B}^{n}]}_{\mathbb{H}_{eq}^{n+1}} + \mathbb{H}_{neq}^{n+1}.\end{aligned} \tag{19}$$

The three time-dependent magneto-elastic stiffness moduli tensors $\mathcal{A}, \mathcal{C}, \mathcal{K}$ are defined in Eq. (10). Now the non-equilibrium parts, both for the stress and magnetic field, have to be derived. We assume that the non-equilibrium parts of the stress and the magnetic field will be derived from the viscoelastic parts of the coupled free energy function presented in Eq. (6), i.e. the dissipative magneto-mechanical coupled stress is

$$\begin{aligned}\boldsymbol{S}_{neq} &= 2\frac{\partial \Omega_{neq}}{\partial \boldsymbol{C}}\\ &= \mu_v[\boldsymbol{C}_v^{-1} - \boldsymbol{C}^{-1}] + \kappa_v \ln J_e \boldsymbol{C}^{-1} + 2r_v \mathbb{B}_e \otimes [\boldsymbol{C} \cdot \mathbb{B}_e] + 2r_v[\boldsymbol{C} \cdot \mathbb{B}_e] \otimes \mathbb{B}_e,\end{aligned} \tag{20}$$

and the Lagrangian form of the viscous magnetic field is given as

$$\mathbb{H}_{neq} = \frac{\partial \Omega_{neq}}{\partial \mathbb{B}} = 2q_v \mathbb{B}_e + 2r_v \boldsymbol{C} \cdot \mathbb{B}_e, \tag{21}$$

where $\boldsymbol{C}_v$ and $\mathbb{B}_v$ are mechanical and magnetic internal variables, respectively. To get the current state of the mechanical and magnetic internal variables that are necessary to calculate the dissipative responses in (20) and (21), respectively, the evolution equations shown in Eqs. (7) and (8) need to be integrated.

During successive chain crosslinking in curing, molecular motions of overstress chains (responsible for the viscous overstress) will experience restriction for a free movement. Hence, the relaxation time will increase with curing time or degree of cure. In order to capture the physical observation during viscoelastic curing process, e.g. relaxation, the mechanical relaxation time has to be evolved with curing time. The main difference of the cure-independent evolution equation (8) from the cure-dependent evolution equation (22) is that now the relaxation time $T_v$ is a function of curing time, i.e. $T_v(t)$ rather than a mere constant parameter which will incorporate the cure-dependence of the viscoelastic process to the constitutive assumption. The modified evolution rule for the internal variable $\boldsymbol{C}_v$ of the curing model is now

$$\dot{\boldsymbol{C}}_v = \frac{1}{T_v(t)}[\boldsymbol{C} - \boldsymbol{C}_v]. \tag{22}$$

Since we do not have any clear evidence in the literature how the evolution of the magnetic relaxation time occurs during curing, we restrict it to a constant value, i.e. the evolution equation for the viscous magnetic induction proposed in (7) will be used in the cure-dependent model also

$$\dot{\mathbb{B}}_v = \frac{2\mu_0}{T_m}\left[q_v \boldsymbol{I} + r_v \boldsymbol{C}^2\right][\mathbb{B} - \mathbb{B}_v]. \tag{23}$$

However, any modification for the magnetic and coupled parameters can be inserted easily in Eq. (23) without further alteration of the main framework of the model.

## 5. Modelling curing shrinkage

One pathological but important property of polymer is the occurrence of a volume reduction during the curing process [33]. The formation of chemical cross-links between molecules allows them to come much closer than in the non-bond situation which eventually leads to a denser packing. Thus, assuming constant mass, the polymerisation process causes an increase in the density. Such density increase, hence volume shrinkage, can take values up to 10% depending on the type of polymers that are being cured. This phenomenon, therefore, is responsible for possibly significant tensile stresses within a specimen held at constant length during cure. To introduce the effect of the curing-induced volume shrinkage to the constitutive relation in the pure mechanical curing, the deformation gradient is decomposed into two parts: a stress producing mechanical part and a volume reducing shrinkage part, i.e.

$$\boldsymbol{F} = \boldsymbol{F}_m \boldsymbol{F}_s \quad \text{with } \boldsymbol{F}_s = [1 + \alpha s]^{1/3} \boldsymbol{I}, \tag{24}$$

cf. Lion and Höfer [29]. Here, $\alpha \in [0, 1]$ denotes the degree of cure and $s \leq 0$ is a parameter controlling the magnitude of the shrinkage. A one dimensional version of this approach can be depicted in Fig. 1. For a magneto-mechanically coupled load, we assume that the overall shrinkage during curing is dependent on the degree of cure ($\alpha$) as well as on the magnitude and duration of exposure of the applied magnetic induction $\mathbb{B}$. Hence, a modified version of Eq. (24) becomes

$$\boldsymbol{F} = \boldsymbol{F}_m \boldsymbol{F}_s \quad \text{with } \boldsymbol{F}_s = [1 + \alpha s\{\alpha, \mathbb{B}\}]^{1/3} \boldsymbol{I}. \tag{25}$$

The above formulation is for a purely isotropic magneto-mechanically coupled curing process as in an unfilled polymer. However, in this contribution, we assume the presence of magnetisable particles which are aligned in a preferred direction. Hence,

the reformulated equation will be

$$\boldsymbol{F}_s = [1+\alpha s\{\alpha, \mathbb{B}\}]^{1/3}\left[\boldsymbol{I}-\beta \boldsymbol{a}\otimes\boldsymbol{a}\right]+\beta \boldsymbol{a}\otimes\boldsymbol{a} \tag{26}$$

where $\boldsymbol{a}$ is a unit vector in the alignment direction and $\beta$ is a scaling parameter $0<\beta<1$. To capture the effect of the magnetic load during curing, we define a 'degree of exposure' $e$ as

$$e = \int_0^t f(\alpha(\tau))|\,\mathbb{B}(\tau)|\;d\tau, \tag{27}$$

where the function $f$ is defined as

$$f(\alpha) = 1-H(\alpha-1), \tag{28}$$

$H$ being the Heaviside function and $|\,\mathbb{B}(\tau)|$ is the magnitude of the induction vector $\mathbb{B}(\tau)$. The parameter $e$ quantifies the exposure of a sample to the magnetic induction during curing. The definition of the function $f(\alpha)$ ensures that any magnetic induction applied after the sample is fully cured, i.e. $\alpha$ reaches 1, does not add to the degree of exposure.

We define $0<e_1<e_2$ to be two cut-off values of exposure such that when $e$ crosses the threshold $e_1$ it starts increasing the value of the shrinkage parameter $s$ from an initial value of $s_1$. As $e$ reaches the second threshold $e_2$, the maximum possible value of shrinkage $s=s_2$ is reached and no more change in $s$ is possible. This behaviour is modelled by the following functional form

$$s = \frac{s_1+s_2}{2}+\frac{s_2-s_1}{2}\tanh\left(\xi\left[e-\frac{1}{2}[e_1+e_2]\right]\right), \tag{29}$$

where $\xi$ is a scaling constant (Fig. 2). Similar to the multiplicative decomposition in Eq. (1), the following decomposition of the right Cauchy–Green tensor reads:

$$\boldsymbol{C} = \boldsymbol{F}^t\boldsymbol{F} = \boldsymbol{F}_s^t\boldsymbol{F}_m^t\boldsymbol{F}_m\boldsymbol{F}_s := \boldsymbol{F}_s^t\boldsymbol{C}_m\boldsymbol{F}_s, \tag{30}$$

which provides a relation for the magneto mechanical right Cauchy–Green strain as

$$\boldsymbol{C}_m = \boldsymbol{F}_m^t\boldsymbol{F}_m = \boldsymbol{F}_s^{-t}\boldsymbol{C}\boldsymbol{F}_s^{-1}. \tag{31}$$

From the usual thermodynamical argumentation, the corresponding Piola–Kirchhoff stress is obtained to read

$$\boldsymbol{S} = \boldsymbol{F}_s^{-1}\boldsymbol{S}_m\boldsymbol{F}_s^{-t}. \tag{32}$$

## 6. Cure-dependent parameters

One of the main assumptions in developing the constitutive relation is that the material parameters appearing in the model will experience a temporal evolution during curing. The number of material parameters appearing in a curing model is solely dependent on the type of the free energy function chosen for the derivations of the three time-dependent magneto-elastic stiffness moduli tensors defined in Eq. (10). The free energy functions described in Eqs. (5) and (6) have several parameters. Some parameters relate to the pure mechanical contribution to the energy function, some to the magnetic contribution to the energy function while few of them are related with the coupled contribution. In the case of magneto-mechanical curing, we have reasonably chosen the temporal evolution of the mechanical and coupled parameters due to the lack of sufficient experimental data, cf. [22]. One straightforward expression, which is also chosen in our previous contribution [43], for the evolution of these parameters is an exponential saturation function as

$$x(t) = x_0+[x_\infty-x_0]\left[1-\exp(-\kappa_p t)\right], \tag{33}$$

which is being governed by initial and final values $x_0$ and $x_\infty$ of a particular parameter, respectively and $\kappa_p$ is a curvature parameter.

### 6.1. Shear and bulk moduli

For the shear modulus evolution, $x_0$ and $x_\infty$ in Eq. (33) are replaced by initial and final shear moduli $\mu_{in}$ and $\mu_\infty$, respectively, as well as the curvature parameter $\kappa_p$ by $\kappa_\mu$. An illustration of Eq. (33) in the case of shear modulus evolution is plotted in Fig. 3. Once the shear modulus is obtained, the elastic bulk modulus is calculated using a relationship, i.e. $\mu/\kappa=0.1$, which is close to Poisson's ratio of $\nu=0.45$ in the case of small deformations.

### 6.2. Coupled parameters

Several papers [17,20] reported that the coupled magneto-mechanical parameters will evolve exponentially. We can take a similar approach as in the case of the mechanical material parameters, e.g. the shear modulus. In the case of the coupled magnetic shear modulus $r(t)$, the two values in Eq. (33), i.e. $x_0$ and $x_\infty$, are replaced by an initial and a final cut-off value $r_0$ and $r_\infty$, respectively, as well as the curvature parameter $\kappa_p$ by $\kappa_r$. To the best of the authors' knowledge, there is no literature which describes the evolution behaviour of other parameters connected to the magnetic variable in a chosen energy function. Henceforth, for simplicity, these parameters can be taken as mere constants. For the energy function expressed in Eq. (5), only one magnetic parameter related to the magnetic part of the energy function is taken as a constant in all simulations presented in Section 7.

### 6.3. Relaxation time

In polymer micromechanics, it is assumed that two types of chains constitute the total polymer networks, i.e. a ground state network and an overstress free network, whereby the second type

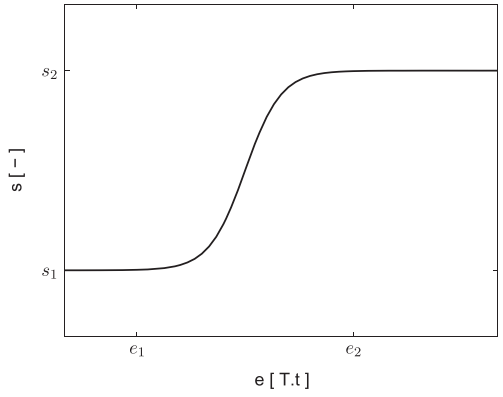


**Fig. 2.** Influence of magnetic induction-dependent parameter $e$ on curing-induced shrinkage parameter $s$.

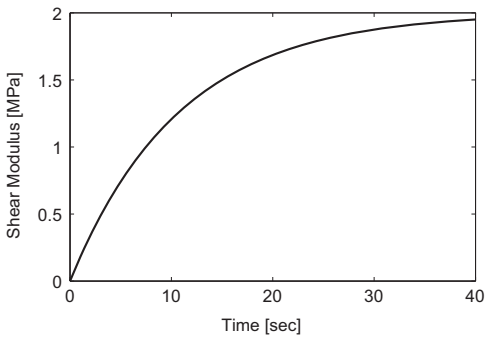


**Fig. 3.** Evolution of the shear modulus $\mu(t)$ with $[\mu_{in}, \mu_\infty, \kappa_\mu] = [0.0001\ \mathrm{N/mm^2}, 2.0\ \mathrm{N/mm^2}, 0.0925\ \mathrm{s^{-1}}]$.

of network is responsible for the stress relaxation, cf. [1]. Due to the chain crosslinking during curing, the overstress dangling chains will get resistance which will be a cause for a longer relaxation time. Therefore, the relaxation time will increase with the curing time or the degree of cure. The relaxation time $T_v$ in Eq. (22) is assumed to evolve according to an exponential saturation function as in Eq. (33). Therein, $x_0$ and $x_\infty$ are substituted by the initial and final relaxation times, i.e. $T_{v0}$ and $T_{v\infty}$, respectively. Moreover, $\kappa_p$ is replaced by $\kappa_\tau$ which describes the reduction rate of the viscosity during curing, i.e. the decrease of the untangling velocity of the chains.

## 7. Numerical examples

In this section, we present some numerical examples to show the capability of the proposed cure dependent magneto-viscoelastic model. To obtain current states for the total stress as well as for the magnetic field the relations in Eqs. (12) and (13) need to be integrated. For simplicity, we use an Euler-backward type implicit integrator resulting in the following updates for the algorithmic stress as

$$\boldsymbol{S}^{n+1} = \boldsymbol{S}^{n}_{eq} + \tfrac{1}{2}\boldsymbol{\mathcal{A}}^{n+1} : [\boldsymbol{C}^{n+1} - \boldsymbol{C}^{n}] + \boldsymbol{\mathcal{C}}^{n+1} \cdot [\mathbb{B}^{n+1} - \mathbb{B}^{n}] + \boldsymbol{S}^{n+1}_{neq}, \tag{34}$$

and the algorithmic magnetic field vector as

$$\mathbb{H}^{n+1} = \mathbb{H}^{n}_{eq} + \tfrac{1}{2}\boldsymbol{\mathcal{C}}^{t,n+1} : [\boldsymbol{C}^{n+1} - \boldsymbol{C}^{n}] + \boldsymbol{\mathcal{K}}^{n+1} \cdot [\mathbb{B}^{n+1} - \mathbb{B}^{n}] + \mathbb{H}^{n+1}_{neq}. \tag{35}$$

In Eqs. (34) and (35), $[\bullet]^n = [\bullet](t_n)$, $t_{n+1} = t_n + \Delta t$ and $\Delta t$ is a time step. The deformation gradient $\boldsymbol{F}$ (hence $\boldsymbol{C}$) and the magnetic induction vector $\mathbb{B}$ are input variables for the mechanical and magnetic load cases, respectively. In updating the stress and the magnetic field, the actual magneto-elastic (equilibrium) stiffness moduli tensors $\boldsymbol{\mathcal{A}}^{n+1}, \boldsymbol{\mathcal{C}}^{n+1}, \boldsymbol{\mathcal{K}}^{n+1}$ at time $t_{n+1}$ are obtained from the generalised Mooney–Rivlin type energy function given in Eq. (5). Detailed derivations for the stiffness moduli tensors are explained in Appendix A. All numerical examples presented in this section correspond to uniaxial deformations of an MRE with the magnetic field applied in the direction of deformation during curing. The deformation gradient can be represented in the form $\boldsymbol{F} = \mathrm{diag}(\lambda_1, \lambda_2, \lambda_2)$ while the magnetic induction is given as $\mathbb{B} = \{B_1, 0, 0\}^t$. Therefore, the constitutive relations for updating the stress tensor and the magnetic field vector elaborated in Sections 3 and 4 need to be formulated in a one-dimensional form.

The time-integration for the mechanical and magnetic evolution equations presented in (22) and (23) for the mechanical and magnetic internal variables, $\boldsymbol{C}_v$ and $\mathbb{B}_v$, respectively, is performed using a standard ordinary differential equation (ODE) solver `ode45` from `Matlab` that employs a higher order explicit Runge–Kutta integration scheme. Further, we need to establish a relation between the stretch in the loading direction $\lambda_1$ and the stretch in the other two transversal directions $\lambda_2$ ($=\lambda_3$). Note that since the elongation is only in one direction, the specimen will contract in the transversal directions and due to the stress-free boundary conditions, both lateral components of the nominal stress $\boldsymbol{P} = \mathrm{diag}(P_{11}, P_{22}, P_{33})$, i.e. $P_{22}$ and $P_{33}$ are zero and only component $P_{11}$ needs to be determined. Using this stress-free boundary condition in the transversal directions, a relation between $\lambda_1$ and $\lambda_2$ is established, see Appendix B for details. In this section, several numerical experiments are performed to obtain the corresponding numerical solutions. The following baseline numerical values of the material parameters are used unless otherwise stated to have a different value for individual computation, see Otténio et al. [11] and Saxena et al. [38]

$$\alpha_e = 0.1, \quad m_e = 1\,\mathrm{T}^2, \quad \chi = 0.5, \quad \mu_0 = 4\pi \times 10^{-7}\,\mathrm{N/A}^2, \quad q = 1/\mu_0,$$
$$\mu_v = 5 \times 10^5\,\mathrm{MPa}, \quad q_v = 5/\mu_0, \quad r_v = 1/\mu_0. \tag{36}$$

### 7.1. Examples without shrinkage effects

In the following section, several numerical examples are presented by considering both magneto-elastic and magneto-viscoelastic models. Numerical examples under shrinkage effects are illustrated in Section 7.3.

#### 7.1.1. Pull–hold–pull loading

In addition to the material parameters listed in Eq. (36), a few more material parameters used for the simulations are described in Table 1.

At first we want to verify whether the developed cure-dependent magneto-viscoelastic model can capture a few important phenomena that occur during the curing process, i.e. the stiffness gain due to the continuous chain crosslinking with an advancement of time and the stress relaxation during a holding period under a purely mechanical or a purely magnetic load. Moreover, we want to check if the model can provide a correct behaviour in the case when the mechanical strain rate becomes zero and/or the magnetic induction rate is zero. For all these cases, simple uniaxial tension tests are performed with a three-step loading, i.e. *pull–hold–pull*, cf. Fig. 4. Unless stated otherwise, for all loading cases, an exponential saturation function for the evolution of the shear modulus $\mu(t)$ and also for the coupled parameter $r(t)$ is used as depicted in Fig. 3. The three phase deformation for the case of a purely mechanical loading (where $\mathbb{B} = \boldsymbol{0}$) consists of a linear increase of the stretch to $\lambda = 1.25$ within the first twenty seconds which is followed by hundred sixty seconds holding and another linear increase of the stretch to $\lambda = 1.5$ during the last twenty seconds, cf. Fig. 4(a). The mechanical stress response, if we evaluate the model only with the elastic part as formulated in Eqs. (14) and (15), is depicted in Fig. 5. Fig. 5(a) shows the mechanical stress over curing time indicating the stress increment in the second deformation phase (during 181–200 s) is higher than the first deformation phase (0–20 s). It is more vivid if we plot the mechanical stress over stretch which basically illustrates the stiffness gain during the holding time, cf. Fig. 5(b). Moreover, the model can capture the physical phenomenon upon which it is based, i.e. if the mechanical strain rate becomes zero and/or the magnetic induction rate is zero, there are no increments in total stress and in magnetic field, cf. Fig. 5(a) and Fig. 6(a), respectively.

To test the model for the pure mechanical stress relaxation process, the three-phase pure mechanical loading as in Fig. 4(a) is applied again. In the case of the magneto-viscoelastic model, the resulting mechanical stress response is plotted in Fig. 7(a) which

**Table 1**
Various baseline material parameters: $\mu_{in}$, $\mu_\infty$ in [MPa]; $\kappa_\mu$ in [MPa$^{-1}$]; $r_0$, $r_\infty$ in [A$^2$/N]; $\kappa_r$ in [N/A$^2$], $T_{v0}$, $T_{v\infty}$, $T_m$ in [s]; $\kappa_\tau$ in [s$^{-1}$].

| $\mu_{in}$ | $\mu_\infty$ | $\kappa_\mu$ | $r_0$ | $r_\infty$ | $\kappa_r$ | $T_{v0}$ | $T_{v\infty}$ | $\kappa_\tau$ | $T_m$ |
|---|---|---|---|---|---|---|---|---|---|
| 1.0e−11 | 2.5e+05 | 0.0255 | 1.0e−10 | $1/\mu_0$ | 0.0255 | 1.0e−10 | 10.0 | 0.0255 | 40 |

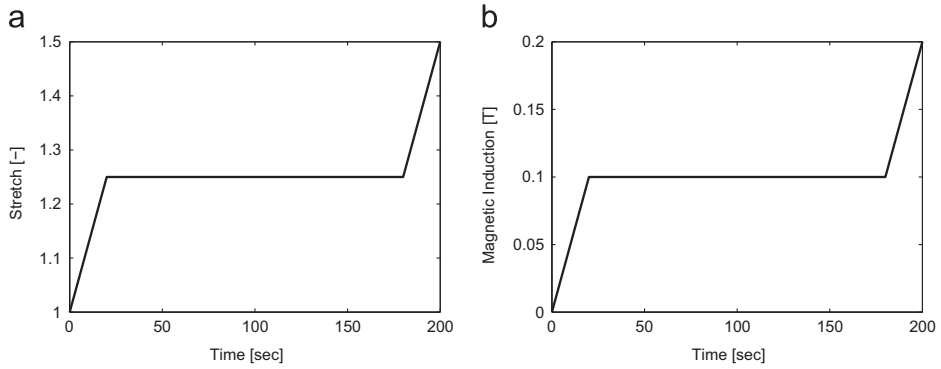


**Fig. 4.** Three-phase loading, i.e. *pull–hold–pull*: (a) mechanical stretch over curing time, (b) magnetic induction over curing time.

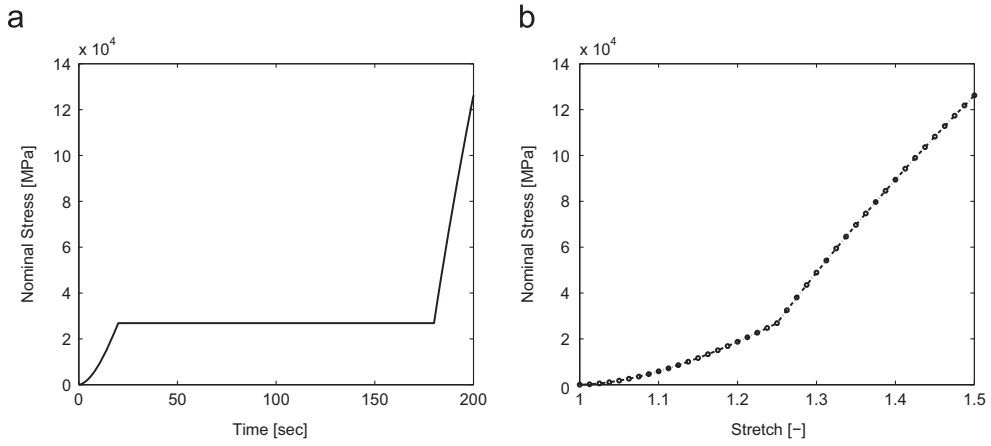


**Fig. 5.** Magneto-elastic curing model with the three phase mechanical loading: (a) mechanical stress over curing time, (b) mechanical stress vs stretch that highlights stiffness gain. The stress response is higher in the second loading phase compared to the first one due to stiffness gain in the longer holding period (21–180 s).

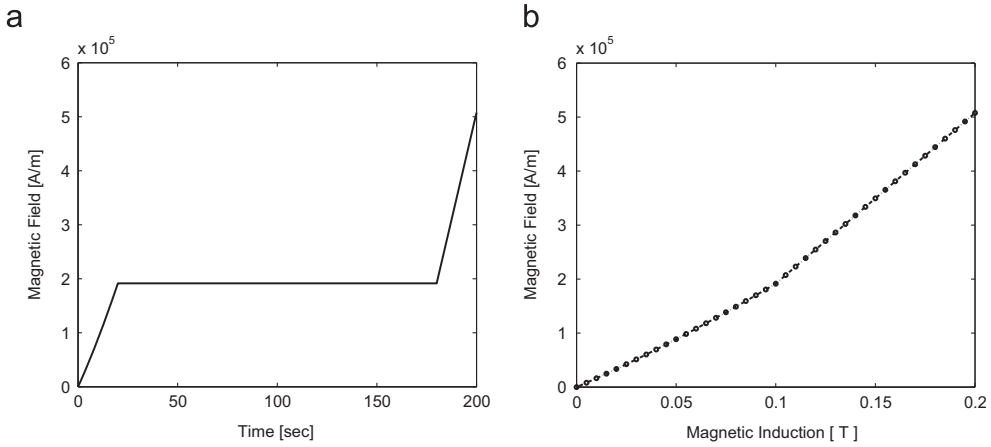


**Fig. 6.** Magneto-elastic curing model with the three phase magnetic loading: (a) Magnetic field over curing time, (b) magnetic field vs magnetic induction that highlights stiffness gain under chain cross-linking where the magnetic stress response is higher in the second loading phase compared to the first one due to stiffness gain in the longer holding period (21–180 s).

indicates that the stress increment in the second deformation phase is higher than the first phase while the stress developed in the first deformation phase relaxes during the holding phase of no load increment (strain rate is zero). Due to the continuous chain crosslinking, more stiffness gains during the holding period of a longer time (one hundred sixty seconds) that reflects in the second phase of loading. If we plot the mechanical stress over mechanical stretch, a kink in Fig. 7(b) indicates a stress relaxation during the holding period.

Now the model can be verified with a pure magnetic loading. For this, a three-phase magnetic loading (in a pure magnetic loading $\lambda_1=\lambda_2=\lambda_3=1.0$) with a linear increase of the magnetic induction to $B_1=0.1$ T within the first twenty seconds which is followed by hundred sixty seconds holding and another linear increase of the induction to $B_1=0.2$ T during the last twenty seconds, cf. Fig. 4(b). In the case of the magneto-elastic model as formulated in Eqs. (14) and (15), the magnetic field response over time (Fig. 6(a)) shows that the magnetic field produced from the second step magnetic load increment is much higher than in the first load step. We plot the magnetic field over the magnetic induction as in Fig. 6(b) which shows the magnetic stiffness gain during the longer holding period. If we compare Fig. 5(b), with

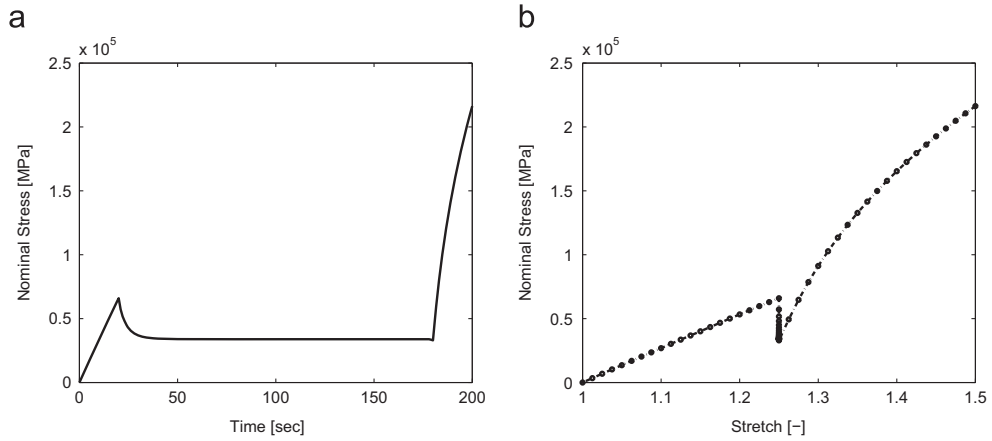


**Fig. 7.** Magneto-viscoelastic curing model with the three phase mechanical loading: (a) mechanical stress over curing time, (b) mechanical stress vs stretch with a stress relaxation during holding time. The mechanical stress response is higher in the second loading phase compared to the first one due to stiffness gain in the longer holding period.

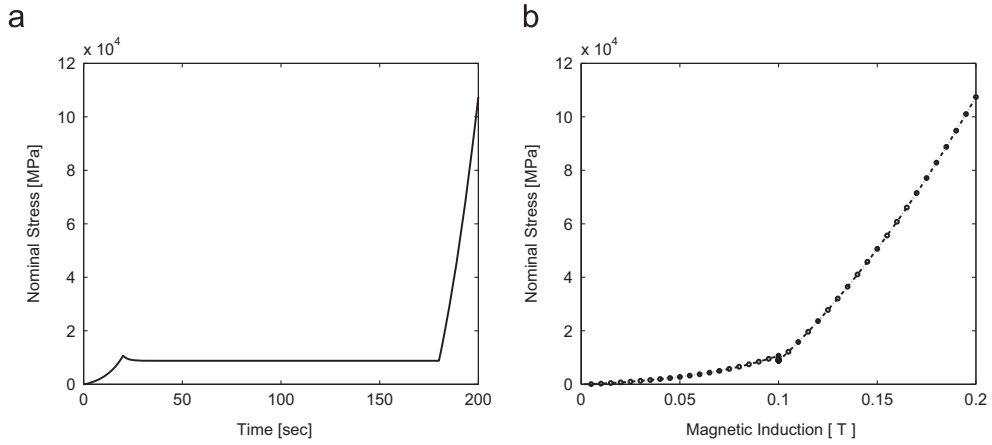


**Fig. 8.** Magneto-viscoelastic curing model with the three phase magnetic loading: (a) mechanical stress over curing time demonstrating a small but quick mechanical stress relaxation, (b) mechanical stress over magnetic induction that highlights a stiffness gain under chain cross-linking where a kink during holding time indicates mechanical stress relaxation.

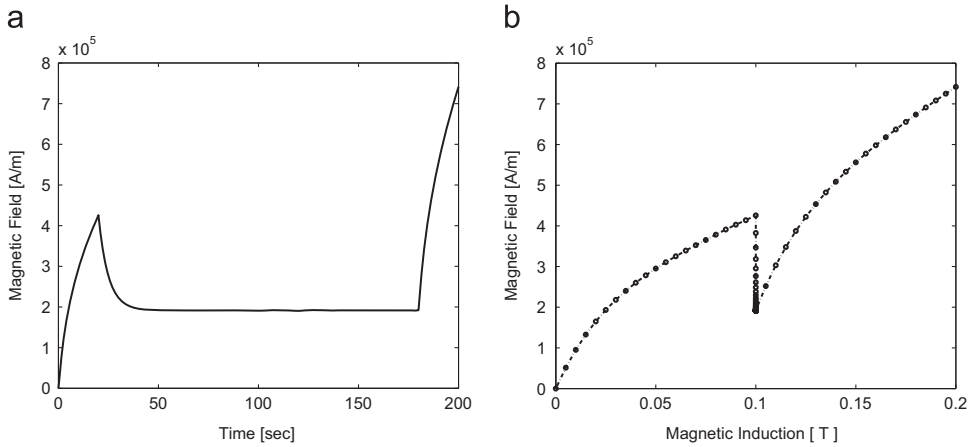


**Fig. 9.** Magneto-viscoelastic curing model with the three phase magnetic loading: (a) magnetic field over curing time with a quick relaxation phenomenon in the holding phase, (b) magnetic field vs magnetic induction that highlights a stiffness gain due to the chain cross-linking where a kink during holding time indicates magnetic field/stress relaxation.

Fig. 6(b), it can be observed that the stiffness gain in the case of magnetic load, cf. Fig. 6(b), is not the same as in the mechanical case, cf. Fig 5(b). Since the coupled parameter linked to the magnetic variable, i.e. $q(t)$, is taken as constant, the magnetic field response is not much more pronounced in the second loading phase.

To test the influence of a magnetic load on the total stress, the three-phase load is once again applied in the magneto-viscoelastic model. As a result of the magneto-mechanical coupled formulation of the model in Eqs. (18) and (19), a magnetic field is created as well as total stresses are developed due to the applied magnetic loading. The total stresses with respect to the time and the

magnetic induction are plotted in Fig. 8(a) and (b), respectively, while the magnetic fields over curing time and magnetic induction are plotted in Fig. 9(a) and (b), respectively. Note that the total stress produced from the second step magnetic load is much higher than in the first deformation step, cf. Fig. 8(a). The reason is that the mechanical parameters such as the shear and the bulk moduli are experiencing a temporal evolution while one of the coupled parameters is kept constant for simplicity. It can be evolved and incorporated easily in the model framework depending on experimental results. There is a small and quick drop of the total stress in the case of the second magnetic load step, i.e. in the holding phase, cf. Fig. 8(a). In contrary, if we plot the magnetic field over curing time, it shows a pronounced response both in the first and in the second magnetic load phases. In the case of the magneto-viscoelastic model, the magnetic field relaxation is profound and quick as compared to the mechanical loading case, cf. Fig. 7(a). The magnetic field increases more in the second load phase and the stress relaxes quickly during the holding period since the magnitude of the magnetic relaxation time is smaller compared to the mechanical relaxation time. We plot the magnetic field over the magnetic induction as in Figs. 8(b) and 9(b), which show the magnetic stiffness gains during the holding period with kinks that reflect magnetic field relaxations during that period (21–180 s).

#### 7.1.2. *Pull–hold–pull–hold loading*

In this section, the effect of the chain crosslinking on the viscous processes needs to be verified with the model developed in Section 4. To demonstrate the effects that arise if also the viscoelastic properties are evolving, the above stretch history is extended to two linear loading phases of ten seconds duration which are interleaved with two holding phases each lasting for ninety seconds, i.e. four phase loading, cf. Fig. 10. It is extended for the both load cases, i.e. mechanical and magnetic loads. We term it as the *pull–hold–pull–hold* loading. For the evolution of the relaxation time, the exponential type saturation function as depicted in Fig. (3) is chosen. In this test, the material parameters listed in Eq. (36) and in Table 1 are utilised.

The four-phase mechanical deformation for the case of the purely mechanical loading consists of a linear increase of the stretch to $\lambda = 1.25$ within the first ten seconds which is followed by ninety seconds holding and a linear increase of the stretch to $\lambda = 1.5$ for another ten seconds and then finally a holding period for ninety seconds, cf. Fig. 10(a). A four-phase purely mechanical loading is applied, cf. Fig. 10(a) while the resulting mechanical stress response over time is plotted in Fig. 11(a). The mechanical stress response plotted in Fig. 11 clearly indicates the desired deceleration of viscous relaxation processes for the model since the equilibrium stresses are reached much later within the second holding phases. Furthermore, slower relaxation time evolutions are also correctly captured as can be observed from the higher stress peaks at the end of each loading phase. In addition to the relaxation process, the developed cure-dependent magneto-viscoelastic model can capture two previously mentioned important phenomena, i.e. the stiffness gain due to the continuous chain crosslinking with the advancement of time and the stress relaxation during the holding period under purely mechanical loads.

To test the influence of the curing process on the magnetic relaxation phenomenon as well as to verify the above-mentioned two important phenomena in the case of a purely magnetic loading, a four-phase magnetic loading is applied. In the four-phase magnetic loading, a linear increase of the magnetic induction to $B_1 = 0.1$ T within the first ten seconds which is followed by ninety seconds holding and another linear increase of the induction to $B_1 = 0.2$ T for ten seconds and then finally a holding period for ninety seconds, cf. Fig. 10(b), is applied. For this numerical test, the parameter $q(t)$ is kept as a constant while the magneto-mechanically coupled parameter $r(t)$ will be evolved following the shape of an exponential saturation function that is depicted qualitatively in Fig. 3. The magnetic field produced by a four-phase purely magnetic loading is plotted in Fig. 12(a), while the resulting magnetic field over magnetic induction is shown in Fig. 12(b). Both figures illustrate the magnetic stiffness gain during the curing process with a quick relaxation phenomenon, cf. Fig. 12(a). Note that in the case of the magnetic relaxation time $T_m$, we restrict ourselves to a non-evolving character, i.e. it is a constant material parameter. Therefore, the amount of relaxation in both holding phases is the same, i.e. during 11–100 s and 111–200 s.

### 7.2. *Shear tests*

In this numerical example, a magnetic induction $\mathbb{B}$ and a stretch $\lambda$ are applied while $\lambda_2$ is held constant at unity. For such a deformation mode, in a three-dimensional setting, the complete deformation gradient reads $\boldsymbol{F} = \lambda_1 \boldsymbol{e}_1 \otimes \boldsymbol{e}_1 + \lambda_2 \boldsymbol{e}_2 \otimes \boldsymbol{e}_2 + \lambda_3 \boldsymbol{e}_3 \otimes \boldsymbol{e}_3 = \lambda \boldsymbol{e}_1 \otimes \boldsymbol{e}_1 + \boldsymbol{e}_2 \otimes \boldsymbol{e}_2 + \lambda_3 \boldsymbol{e}_3 \otimes \boldsymbol{e}_3$, where $\boldsymbol{e}_i$ $(i = 1, 2, 3)$ are the orthonormal unit vectors. The magnetic induction is applied at an angle $\phi$ to the direction $\boldsymbol{e}_1$ while the applied stretch $\lambda$ aligns with the first orthonormal direction $\boldsymbol{e}_1$. As a result of the applied loads, the principal directions of the stress will be at an angle $\vartheta_s$ to the Cartesian basis vector $\boldsymbol{e}_1$ as depicted in Fig. 13. For the compressible type model as presented in Section 2, the unknown stretch quantity $\lambda_3$ is calculated iteratively assuming a plane stress condition, i.e. $\sigma_{33} = 0$. A concise recipe for derivations and solutions of the resultant non-linear equations in the case of the uniaxial tension mode is described in Appendix B.

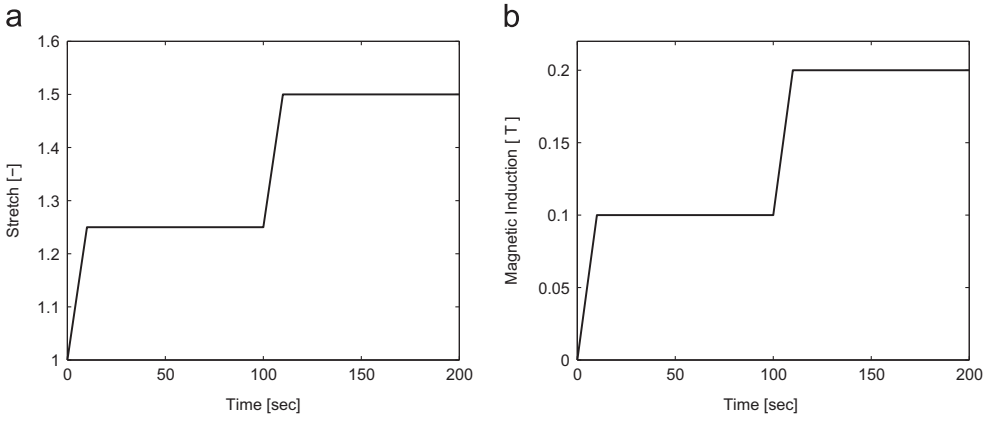


**Fig. 10.** Four-phase loading: (a) mechanical stretch over curing time, (b) magnetic induction over curing time.

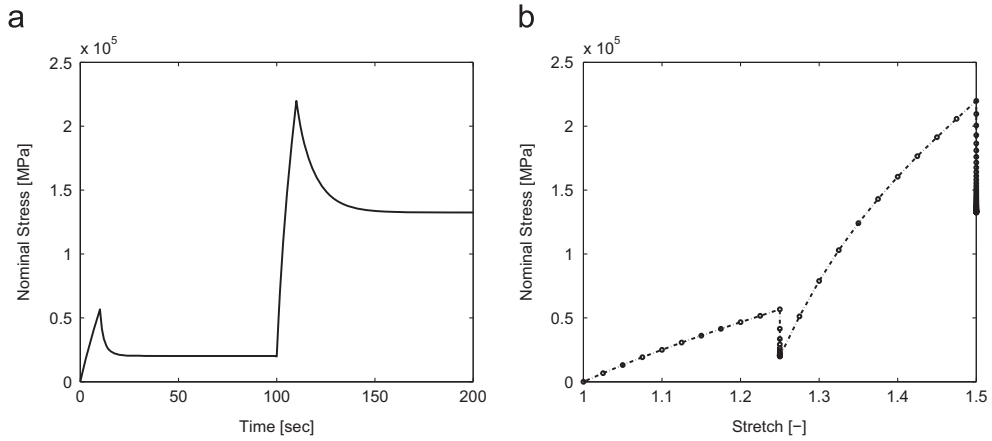


**Fig. 11.** Magneto-viscoelastic curing model with the four phase mechanical loading: (a) purely mechanical stress over curing time as produced from a four-phase purely mechanical loading, (b) purely mechanical stress vs stretch that highlights stiffness gain in successive loading phases. The stress relaxation is decelerated in the second holding phase due to a time-evolving characteristics of the mechanical relaxation parameter, $T_v$.

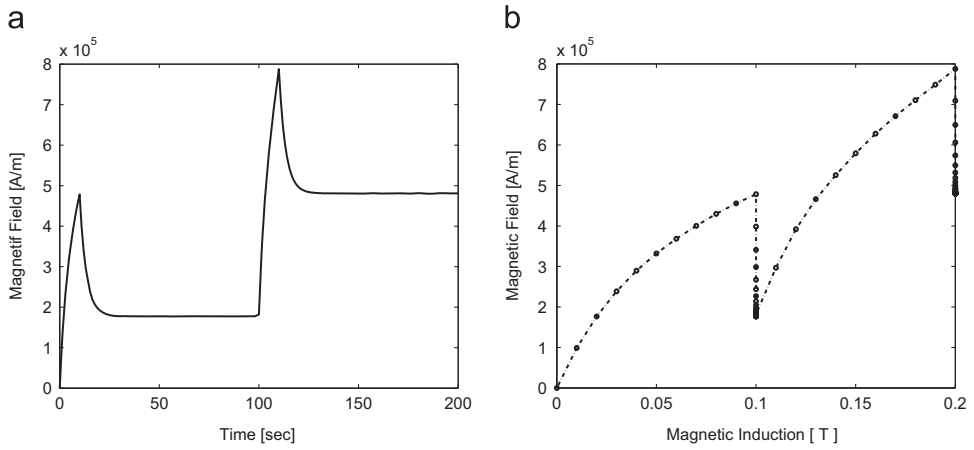


**Fig. 12.** Magneto-viscoelastic curing model with the *pull–hold–pull–hold* magnetic loading: (a) magnetic field over curing time, (b) magnetic field vs magnetic induction that highlights stiffness gain due to a continuous chain crosslinking. However, the stress relaxation in the two holding phases is the same due to a constant value of the magnetic relaxation parameter, $T_m$.

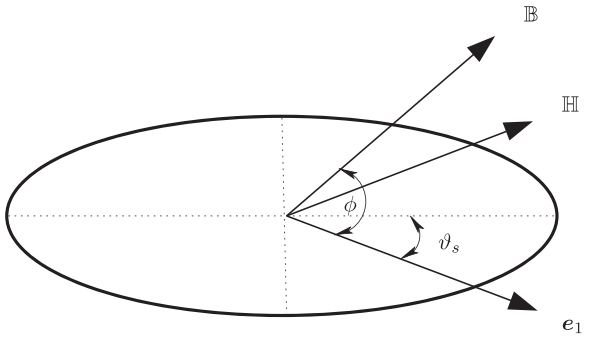


**Fig. 13.** An ellipse illustrates the principal directions of total Cauchy stress $\sigma$ as its principal axes while respective alignments of magnetic induction $\mathbb{B}$, magnetic field $\mathbb{H}$ and Cartesian direction $e_1$.

All subsequent computations are performed for a magnitude of the magnetic induction $|\mathbb{B}| = 0.4\,\mathrm{T}$. It is assumed that the magnetic induction is applied earlier than the curing process starts. Hence, the material seems to be pre-magnetised with the magnetic induction which helps to diminish the magnetic viscous effects when we start to count the time of loading and curing at $t=0$. In addition to the magnetic load, we apply a mechanical stretch at $t=0$ at a linearly increasing and decreasing magnitude of a constant slope of $5.0 \times 10^{-3}\,\mathrm{s}^{-1}$ while the maximum applied stretch after 100 s is 1.5 (total time of loading and unloading phases is 200 s). In addition to the parameters depicted in Eq. (36), the parameters listed in Table 2 are used. In this case $q$ and $\mu_v$ are set to $10/\mu_0$ and 1.0e+3, respectively.

It is illustrated in Fig. 14 (a) that the maximum principal Cauchy stress $\sigma_{\max}$ rises and falls following a similar pattern as the applied stretch $\lambda$. The rise of the stress in the increasing phase is more non-linear compared to the decreasing phase since various material parameters evolve mostly in the increasing phase. The shape of the unloading stress with time is essentially linear as the material is almost cured in this phase. Moreover, a small amount of compressive stress develops when we try to fully unload the material since the material becomes stronger in the meantime. Such a compressive stress is absent in the case of a fully cured anisotropic viscoelastic model, see Saxena et al. [40]. Similar to the fully cured model previously proposed by us, the maximum value of the stress reached is higher for a smaller magnitude of the angle $\phi$ and vice versa, i.e. the angle between the first orthonormal direction $\boldsymbol{e}_1$ and the applied magnetic load $\mathbb{B}$.

Due to the evolution of the internal variables in the case of viscoelastic responses, the orientation angle of the principal stress $\vartheta_s$ keeps changing. Starting from a non-zero value, it slightly decreases with respect to time. During the unloading phase as the stretch is gradually reduced from 1.5 to 1.0 within the time span of 100 s, the orientation of the total Cauchy stress changes dramatically, cf. Fig. 14(b). Therefore, we can observe a jump in the magnitude of $\vartheta_s$. Moreover, the value of the angle $\vartheta_s$ is larger in

**Table 2**
Various baseline material parameters: $\mu_{in}$, $\mu_{\infty}$ in [MPa]; $\kappa_{\mu}$ in [MPa$^{-1}$]; $r_0$, $r_{\infty}$ in [A$^2$/N]; $\kappa_r$ in [N/A$^2$], $T_{v0}$, $T_{v\infty}$, $T_m$ in [s]; $\kappa_{\tau}$ in [s$^{-1}$].

| $\mu_{in}$ | $\mu_{\infty}$ | $\kappa_{\mu}$ | $r_0$ | $r_{\infty}$ | $\kappa_r$ | $T_{v0}$ | $T_{v\infty}$ | $\kappa_{\tau}$ | $T_m$ |
|---|---|---|---|---|---|---|---|---|---|
| 1.0e−11 | 2.5e+05 | 0.0255 | 1.0e−10 | $2/\mu_0$ | 0.0255 | 1.0e−10 | 10.0 | 0.0255 | 10 |

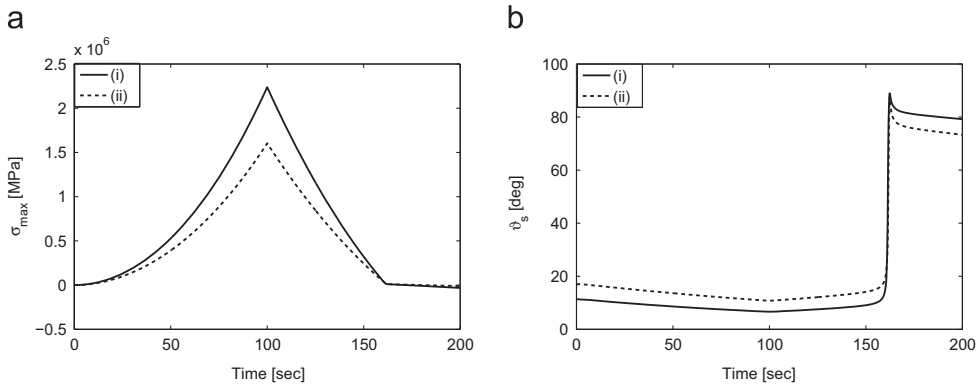


**Fig. 14.** (a) Maximum principal Cauchy stress $\sigma_{\max}$ with time: (i) $\phi=\pi/6$ and (ii) $\phi=\pi/4$. (b) Evolution of the orientation angle $\vartheta_s$: (i) $\phi=\pi/6$ and (ii) $\phi=\pi/4$.

the case of a smaller $\phi$ and vice versa. These results are in line with the simulations performed for a similar deformation mode with a fully cured anisotropic viscoelastic model, e.g., Saxena et al. [40].

### 7.3. Examples with shrinkage effects

Finally the curing process-induced and magnetic-induction-induced shrinkage models proposed in Eq. (5) are illustrated with a few numerical examples. Unless otherwise stated, for all numerical examples presented in this section, the material parameters listed in Table 1 in addition to the parameters in Eq. (36) are utilised. For shrinkage induced stress build-up during cure in the case of a purely mechanical load, the three-phase mechanical loading is again applied, cf. Fig. 4(a). The evolution for the degree of cure $\alpha$ required in Eq. (24) is considered as an exponential saturation function. Such a function is already considered in Eq. (33) and plotted in Fig. 15(a) for the degree of cure evolution. There, the initial and the final values of the degree of cure, i.e. $\alpha_0$ and $\alpha_{\infty}$, are set to $1.0\times10^{-8}$ and 1.0, respectively. The curvature parameter $\kappa_{\alpha}$ is taken as 0.0225 s$^{-1}$ for a two hundred seconds curing time. A total curing-induced volume reduction of 5% is considered, i.e. $s=-0.05$. For a three-phase pure mechanical loading ($s$ does not depend on the magnetic load $\mathbb{B}$), the stress response without the curing shrinkage is plotted with a solid line while the same response considering a curing shrinkage is depicted by the dotted line in Fig. 15(b). The shrinkage-induced total stress is higher than the purely mechanical stress since both the mechanical load and the shrinkage-generated load contribute to the stress development.

To illustrate the influence of a magnetic load for the curing-induced volume shrinkage, the magnetic-induction-dependent curing model systematically formulated in Eq. (26) is utilised now. In this case, a three-phase magneto-mechanical coupled load is applied, cf. Fig. 4. At first, in order to see how a magneto-mechanical load generates shrinkage-induced stress, we assume that the shrinkage parameter does not depend on the magnetic load $\mathbb{B}$, i.e. there is no direct coupling between $s$ and $\mathbb{B}$. For this, in the presence of the load, the shrinkage-generated stress is plotted in Fig. 16(b) with a solid line. To consider the influence of a magnetic load via coupling with $s$, we have to determine the parameter degree of exposure, $e$, for the three-phase magnetic load. According to Eq. (29), the shrinkage controlling parameter $s$ is not simply a constant but depends on the degree of exposure $e$. Therefore, for the three-phase magnetic load the dependence of $s$ is calculated and plotted in Fig. 16(a). For this calculation, different cut-off values expressed in Eq. (29) are $[s_1, s_2, e_1, e_2, \xi, \beta] = [0.0, 0.05, 0.0\ \mathrm{T\,s}, 15.0\ \mathrm{T\,s}, 0.5, 0.5]$. Using the current value of $s$, which accounts for the magnetic-induction dependence on the curing-generated shrinkage, the stress response is depicted in Fig. 16(b) by a dot-dash line for a purely isotropic shrinkage while the direction-dependent shrinkage response with a direction vector $\boldsymbol{a}=[1,0,0]$ is presented by a dotted line. Since the particle alignments are in the load direction which hinders a sample to shrink, the total shrinkage-generated stress is less compared to a purely isotropic case. It shows that the magnitude and the duration of exposure of the magnetic load affects the total shrinkage generated stress. This makes a material stiffer which might be one cause for a more pronounced shrinkage-induced stress generation during a curing process. For all examples presented in this section, only the elastic part of the magneto-mechanical curing models is considered. Note that more sophisticated approaches for the evolution of $\alpha$, as mentioned, e.g. in [21], are not considered here for the sake of simplicity but are, nonetheless, straightforward to incorporate.

## 8. Conclusion and outlook

In this contribution we propose a three-dimensional magneto-viscoelastic constitutive framework that can model the stiffness gain during a curing process undergoing finite deformations. Moreover, it includes a novel magnetic induction-dependent volume shrinkage model based on a multiplicative decomposition of the deformation gradient. The novel constitutive framework obeys relevant laws of thermodynamics. The finite strain model is in line with our earlier proposed hypoelastic type approach that was formulated mainly for a pure mechanical curing process. Based on some elementary rheological considerations the constitutive equations are derived. Several homogeneous numerical

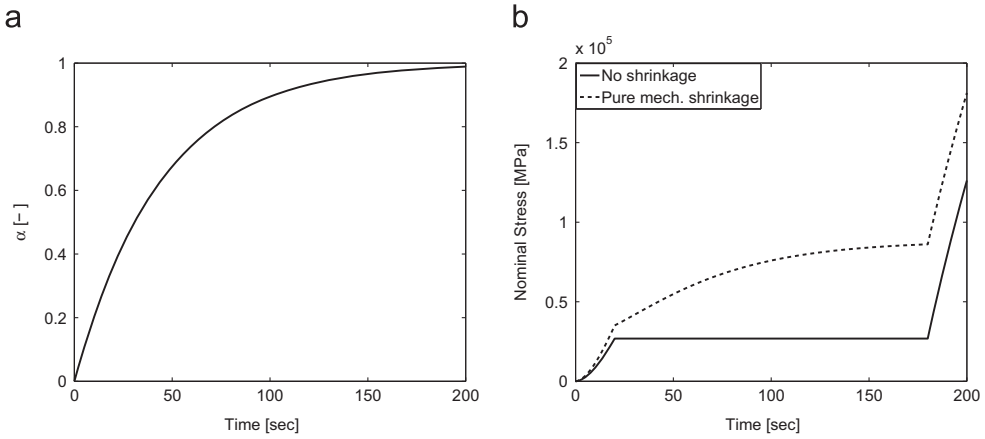


**Fig. 15.** Shrinkage-induced stress development under a three phase mechanical loading: (a) degree of cure using an exponential saturation function, (b) shrinkage-induced stress responses for the three-phase purely mechanical load.

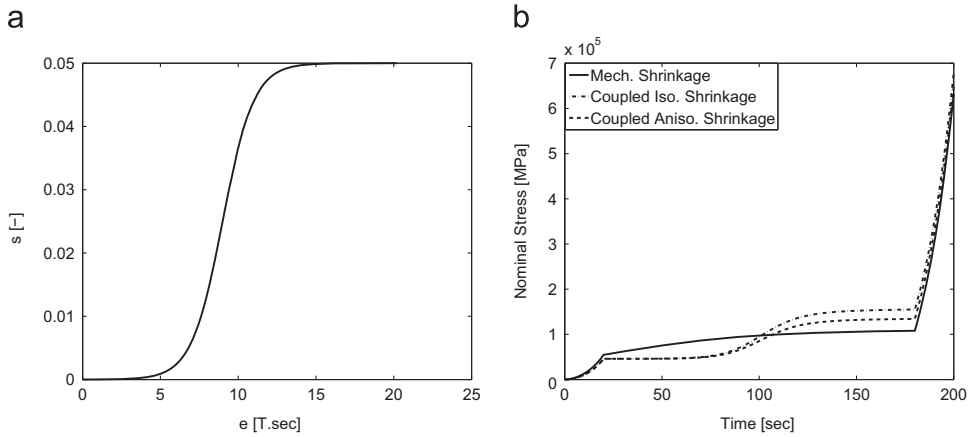


**Fig. 16.** Magnetic-load-dependent shrinkage model: (a) degree of exposure *e* results from the three-phase magnetic load, (b) magnetic-induction-dependent shrinkage-generated stress responses for the three-phase magneto-mechanical load.

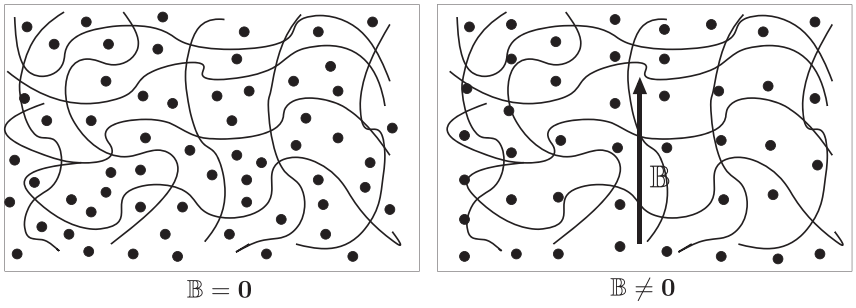


**Fig. 17.** Particles alignment during curing: (I) in the absence of a magnetic load, isotropic material; (II) preferred direction in the presence of a magnetic field.

tests are performed which show that the framework can capture relevant phenomena expected in a magneto-mechanical coupled curing process. The purely phenomenological character of the presented approach can be investigated further aiming to develop a fully micro-mechanically based magneto-viscoelastic curing model. Some polymer curing reactions are exothermal processes. Therefore, an extension to incorporate the thermal influence during curing is going to be dealt with in a future work. In order to simulate complicated and more realistic boundary value problems, the model is required to be implemented in a magneto-mechanically coupled finite element framework. Additionally, there is a plan to perform parameter identifications as well as validation of the model with real experimental data.

## Acknowledgements

This work is funded by an ERC Advanced Grant within the Project MOCOPOLY (Project No. 289049).

## Appendix A

In deriving the three stiffness moduli expressed in Eq. (10), a free energy function that is utilised in modelling a fully cured magneto-sensitive elastomer is required. However, in the cure-dependent modelling the material parameters appearing in the energy function will be time-dependent parameters instead of merely some material constants. If one considers a simplified situation, the energy function will end up in a concise format, i.e. the curing material has a preferred direction due to an alignment of the ferromagnetic particles. We can assume that the direction of the chain alignment is given in the reference configuration by a unit vector $\mathbf{a}$. On application of a magnetic induction $\mathbb{B}$, there are two preferred directions. For such a material, the energy density function $\Omega=\tilde{\Omega}(\boldsymbol{F},\mathbb{B},\mathbf{a})$ can be specified in the form of ten linearly independent scalar invariants, cf. Spencer [41]. In our case, we choose the invariants to be

$$I_1=\operatorname{tr}\boldsymbol{C},\quad I_2=\tfrac{1}{2}\left[I_1^2-\operatorname{tr}\boldsymbol{C}^2\right],\quad I_3=\det\boldsymbol{C},\quad I_4=\mathbb{B}\cdot\mathbb{B},$$
$$I_5=\mathbb{B}\cdot[\boldsymbol{C}\mathbb{B}],\quad I_6=[\boldsymbol{C}\mathbb{B}]\cdot[\boldsymbol{C}\mathbb{B}],\quad I_7=\mathbf{a}\cdot[\boldsymbol{C}\mathbf{a}],\quad I_8=[\boldsymbol{C}\mathbf{a}]\cdot[\boldsymbol{C}\mathbf{a}],$$
$$I_9=\mathbf{a}\cdot\mathbb{B},\quad I_{10}=\mathbf{a}\cdot[\boldsymbol{C}\mathbb{B}] \tag{37}$$

where $\boldsymbol{C}=\boldsymbol{F}^t\boldsymbol{F}$ is the right Cauchy–Green strain tensor.

However, in the case of curing of a magnetoelastic polymer in the presence of a magnetic induction, the alignment of the ferromagnetic particles always occurs in the direction of the externally applied magnetic induction, cf. Fig. 17. Thus, the magnetic induction can be written as a scalar multiple of the preferred direction, i.e. $\mathbb{B}=\beta\mathbf{a}$. For the above simplification, we obtain the following relations:

$$I_4=\beta I_9=I_9^2,\quad I_5=I_9^2I_7=I_9I_{10},\quad I_6=I_4I_8. \tag{38}$$

Henceforth, the only linearly independent invariants are $I_1,\ldots,I_6$ and we may consider the energy density to be dependent only on them, i.e. for an unconstrained isotropic material, $\tilde{\Omega}$ is a function of the six invariants $I_1$ through $I_6$, i.e.

$$\Omega=\tilde{\Omega}(\boldsymbol{C},\mathbb{B})=\tilde{\Omega}(I_1,I_2,I_3,I_4,I_5,I_6). \tag{39}$$

Therefore, expressions for the three different time-dependent stiffness tensors defined in Eq. (10) can be expanded in the form below:

$$\mathcal{A}(t)=4\sum_{\zeta=1,\zeta\neq4}^{6}\sum_{\eta=1,\eta\neq4}^{6}\Omega_{\zeta\eta}(t)\frac{\partial I_\zeta}{\partial\boldsymbol{C}}\otimes\frac{\partial I_\eta}{\partial\boldsymbol{C}}+4\sum_{\eta=1,\eta\neq4}^{6}\Omega_\eta(t)\frac{\partial^2 I_\eta}{\partial\boldsymbol{C}\otimes\partial\boldsymbol{C}} \tag{40}$$

$$\mathcal{C}(t)=2\sum_{\zeta=4}^{6}\sum_{\eta=1,\eta\neq4}^{6}\Omega_{\zeta\eta}(t)\frac{\partial I_\zeta}{\partial\mathbb{B}}\otimes\frac{\partial I_\eta}{\partial\boldsymbol{C}}+2\sum_{\eta=5}^{6}\Omega_\eta(t)\frac{\partial^2 I_\eta}{\partial\mathbb{B}\otimes\partial\boldsymbol{C}} \tag{41}$$

$$\mathcal{K}(t)=\sum_{\zeta=4}^{6}\sum_{\eta=4}^{6}\Omega_{\zeta\eta}(t)\frac{\partial I_\zeta}{\partial\mathbb{B}}\otimes\frac{\partial I_\eta}{\partial\mathbb{B}}+\sum_{\eta=4}^{6}\Omega_\eta(t)\frac{\partial^2 I_\eta}{\partial\mathbb{B}\otimes\partial\mathbb{B}} \tag{42}$$

where $\Omega_\eta(t)=\partial\Omega(t)/\partial I_\eta$, $\Omega_{\zeta\eta}(t)=\partial^2\Omega(t)/\partial I_\zeta\partial I_\eta$. At this stage, we need to determine the first and second derivatives of the total energy function $\tilde{\Omega}(t)$ with respect to the six invariants. To this end, expressions for the material independent various tensorial derivatives are required which can be taken from the lecture notes given by Steinmann [42]. The first derivatives of the invariants $I_\eta$ with respect to $\boldsymbol{C}$ and $\mathbb{B}$ can be computed once and for all without specifying the exact format of the total energy $\tilde{\Omega}(t)$. Thus we obtain the following intermediate results:

$$\frac{\partial I_1}{\partial\boldsymbol{C}}=\boldsymbol{I},\quad \frac{\partial I_1}{\partial\mathbb{B}}=\boldsymbol{0}$$
$$\frac{\partial I_2}{\partial\boldsymbol{C}}=I_2\boldsymbol{B}+I_3\boldsymbol{B}^2,\quad \frac{\partial I_2}{\partial\mathbb{B}}=\boldsymbol{0}$$
$$\frac{\partial I_3}{\partial\boldsymbol{C}}=\operatorname{cof}\boldsymbol{C},\quad \frac{\partial I_3}{\partial\mathbb{B}}=\boldsymbol{0}$$
$$\frac{\partial I_4}{\partial\boldsymbol{C}}=\boldsymbol{0},\quad \frac{\partial I_4}{\partial\mathbb{B}}=2\mathbb{B}$$
$$\frac{\partial I_5}{\partial\boldsymbol{C}}=\mathbb{B}\otimes\mathbb{B},\quad \frac{\partial I_5}{\partial\mathbb{B}}=2\boldsymbol{C}\cdot\mathbb{B}$$
$$\frac{\partial I_6}{\partial\boldsymbol{C}}=2[\boldsymbol{C}\cdot\mathbb{B}\otimes\mathbb{B}]^{\mathrm{sym}},\quad \frac{\partial I_6}{\partial\mathbb{B}}=2\boldsymbol{C}^2\cdot\mathbb{B}.$$

Similarly the second order derivatives of the invariants $I_\eta$ with respect to $\boldsymbol{C}$ and $\mathbb{B}$ can be computed once and for all. Thus we obtain the following intermediate results:

$$\frac{\partial^2 I_1}{\partial\boldsymbol{C}\otimes\partial\boldsymbol{C}}=\boldsymbol{0},\quad \frac{\partial^2 I_1}{\partial\mathbb{B}\otimes\partial\mathbb{B}}=\boldsymbol{0}$$
$$\frac{\partial^2 I_2}{\partial\boldsymbol{C}\otimes\partial\boldsymbol{C}}=\mathbb{A}_2,\quad \frac{\partial^2 I_2}{\partial\mathbb{B}\otimes\partial\mathbb{B}}=\boldsymbol{0}$$
$$\frac{\partial^2 I_3}{\partial\boldsymbol{C}\otimes\partial\boldsymbol{C}}=I_3[\boldsymbol{B}\otimes\boldsymbol{B}-\mathbb{I}_{\boldsymbol{B}}^{\mathrm{sym}}],\quad \frac{\partial^2 I_3}{\partial\mathbb{B}\otimes\partial\mathbb{B}}=\boldsymbol{0}$$
$$\frac{\partial^2 I_4}{\partial\boldsymbol{C}\otimes\partial\boldsymbol{C}}=\boldsymbol{0},\quad \frac{\partial^2 I_4}{\partial\mathbb{B}\otimes\partial\mathbb{B}}=2\boldsymbol{I}$$
$$\frac{\partial^2 I_5}{\partial\boldsymbol{C}\otimes\partial\boldsymbol{C}}=\boldsymbol{0},\quad \frac{\partial^2 I_5}{\partial\mathbb{B}\otimes\partial\mathbb{B}}=2\boldsymbol{C}$$
$$\frac{\partial^2 I_6}{\partial\boldsymbol{C}\otimes\partial\boldsymbol{C}}=2[\mathbb{I}_{\boldsymbol{B}}^{\mathrm{sym}}\cdot\mathbb{B}\otimes\mathbb{B}]^{\mathrm{sym}},\quad \frac{\partial^2 I_6}{\partial\mathbb{B}\otimes\partial\mathbb{B}}=2\boldsymbol{C}^2.$$

Moreover, the mixed second order derivatives of the invariants $I_\eta$ with respect to $\boldsymbol{C}$ and $\mathbb{B}$ are obtained as in the following ways:

$$\frac{\partial^2 I_1}{\partial\boldsymbol{C}\otimes\partial\mathbb{B}}=\boldsymbol{0},\quad \frac{\partial^2 I_1}{\partial\mathbb{B}\otimes\partial\boldsymbol{C}}=\boldsymbol{0}$$
$$\frac{\partial^2 I_2}{\partial\boldsymbol{C}\otimes\partial\mathbb{B}}=\boldsymbol{0},\quad \frac{\partial^2 I_2}{\partial\mathbb{B}\otimes\partial\boldsymbol{C}}=\boldsymbol{0}$$
$$\frac{\partial^2 I_3}{\partial\boldsymbol{C}\otimes\partial\mathbb{B}}=\boldsymbol{0},\quad \frac{\partial^2 I_3}{\partial\mathbb{B}\otimes\partial\boldsymbol{C}}=\boldsymbol{0}$$
$$\frac{\partial^2 I_4}{\partial\boldsymbol{C}\otimes\partial\mathbb{B}}=\boldsymbol{0},\quad \frac{\partial^2 I_4}{\partial\mathbb{B}\otimes\partial\boldsymbol{C}}=\boldsymbol{0}$$
$$\frac{\partial^2 I_5}{\partial\boldsymbol{C}\otimes\partial\mathbb{B}}=\mathbb{B}\otimes\boldsymbol{I}+\boldsymbol{I}\otimes\mathbb{B},\quad \frac{\partial^2 I_5}{\partial\mathbb{B}\otimes\partial\boldsymbol{C}}=2\mathbb{B}\cdot\mathbb{I}^{\mathrm{sym}}$$
$$\frac{\partial^2 I_6}{\partial\boldsymbol{C}\otimes\partial\mathbb{B}}=\boldsymbol{A}_6^T,\quad \frac{\partial^2 I_6}{\partial\mathbb{B}\otimes\partial\boldsymbol{C}}=\boldsymbol{A}_6.$$

Here $\boldsymbol{B}=\boldsymbol{C}^{-1}=[\boldsymbol{F}^t\boldsymbol{F}]^{-1}$ and $\mathbb{I}_{\boldsymbol{B}}^{\mathrm{sym}}$ denotes referential fourth-order tensor with coefficients $2[\mathbb{I}_{\boldsymbol{B}}^{\mathrm{sym}}]_{IJKL}=B_{IK}B_{JL}+B_{IL}B_{JK}$. To abbreviate the Hessian of the invariant $I_2$ with respect to the Cauchy–Green strain $\boldsymbol{C}$ we introduced the referential fourth-order tensor $\mathbb{A}_2=I_2[\boldsymbol{B}\otimes\boldsymbol{B}-\boldsymbol{I}_{\boldsymbol{B}}^{\mathrm{sym}}]+2[\boldsymbol{B}^2\otimes\operatorname{cof}\boldsymbol{C}]^{\mathrm{sym}}\quad -I_3[\boldsymbol{B}^2\overline{\otimes}\boldsymbol{B}+\boldsymbol{B}^2\underline{\otimes}\boldsymbol{B}+\boldsymbol{B}\overline{\otimes}\boldsymbol{B}^2+\boldsymbol{B}\underline{\otimes}\boldsymbol{B}^2]$. Moreover, $\mathbb{I}^{\mathrm{sym}}$ denotes referential fourth-order tensor with coefficients $2[\mathbb{I}^{\mathrm{sym}}]_{IJKL}=\delta_{IK}\delta_{JL}+\delta_{IL}\delta_{JK}$. We abbreviated the mixed second derivatives of the invariant $I_6$ by the referential third-order tensor $\boldsymbol{A}_6=2\mathbb{B}\cdot\boldsymbol{C}\cdot\mathbb{I}^{\mathrm{sym}}+2[\boldsymbol{C}\otimes\mathbb{B}]:\mathbb{I}^{\mathrm{sym}}$.

## Appendix B

To establish a relation between $\lambda_1$ and $\lambda_2$, at first we need to discretise the evolution equation (22) by an Euler backward type integration scheme in order to get the current value of the tensor-like internal variable $\boldsymbol{C}_v$, i.e.

$$\frac{\boldsymbol{C}_v^{n+1}-\boldsymbol{C}_v^n}{\Delta t}=\frac{1}{T_v^{n+1}}\left[\boldsymbol{C}^{n+1}-\boldsymbol{C}_v^n\right] \tag{43}$$

which can be rearranged as

$$\boldsymbol{C}_v^{n+1}=\frac{T_v^{n+1}}{T_v^{n+1}+\Delta t}\left[\frac{\Delta t}{T_v^{n+1}}\boldsymbol{C}^{n+1}+\boldsymbol{C}_v^n\right]. \tag{44}$$

This discretised form can be written in a scalar decoupled form

since we apply the mechanical load in a uniaxial mode,

$$\lambda_{2v}^{2,n+1} = \frac{T_v^{n+1}}{T_v^{n+1}+\Delta t}\left[\frac{\Delta t}{T_v^{n+1}}\lambda_2^{2,n+1}+\lambda_{2v}^{2,n}\right] = \left[\frac{\Delta t}{T_v^{n+1}+\Delta t}\lambda_2^{2,n+1}+\frac{T_v^{n+1}}{T_v^{n+1}+\Delta t}\lambda_{2v}^{2,n}\right] \tag{45}$$

where $\lambda_2^2$ and $\lambda_{2v}^2$ are the second diagonal entries of the tensors $\boldsymbol{C}$ and $\boldsymbol{C}_v$, respectively. From Eq. (34), with the help of Voigt notation and applying the condition that the stress $P_{22}$ is zero, we obtain a non-linear relation for the actual value of $\lambda_2$,

$$\begin{aligned} f(\lambda_2) = {} & \left[3\kappa+2\mu-\kappa\lambda^{-2}\lambda^{2,n}\right]\lambda_2^2-2\mu\lambda_2^{2,n}-2\kappa\lambda_2^2\ln(\lambda) \\ & -4\kappa\lambda_2^2\ln(\lambda_2)+2\kappa\lambda_2^{2,n}\ln(\lambda)+4\kappa\lambda_2^{2,n}\ln(\lambda_2)-2\kappa\lambda_2^{2,n} \\ & +2\mu_v\lambda_2^4\left[\frac{\Delta t}{T_v+\Delta t}\lambda_2^2+\frac{T_v}{T_v+\Delta t}\lambda_{2v}^{2,n}\right]^{-1}-2\mu_v\lambda_2^2+2\kappa_v\lambda_2^2\ln(\lambda) \\ & +4\kappa_v\lambda_2^2\ln(\lambda_2)-2\kappa_v\lambda_2^2\ln(\lambda_v) \\ & -2\kappa_v\lambda_2^2\ln\left(\frac{\Delta t}{T_v+\Delta t}\lambda_2^2+2\frac{T_v}{T_v+\Delta t}\lambda_{2v}^{2,n}\right)=0 \end{aligned} \tag{46}$$

where $\lambda^{2,n}, \lambda_{2v}^{2,n}$ and $\lambda_2^{2,n}$ are the stretch values at time $t_n$. This non-linear equation can be solved using an iterative scheme, e.g. Newton method to get the update value of $\lambda_2$. Note that the superscript $n+1$ is omitted for simplicity.

## References


[1] J.C. Bergström, M.C. Boyce, Constitutive modeling of the large strain time-dependent behaviour of elastomers, J. Mech. Phys. Solids 46 (1998) 931–954.
[2] A. Boczkowska, S.F. Awietjan, Smart composites of urethane elastomers with carbonyl iron, J. Mater. Sci. 44 (2009) 4104–4111.
[3] R. Bustamante, A. Dorfmann, R.W. Ogden, A nonlinear magnetoelastic tube under extension and inflation in an axial magnetic field: numerical solution, J. Eng. Math. 59 (2007) 139–153.
[4] R. Bustamante, Mathematical modelling of boundary conditions for magneto-sensitive elastomers: variational formulations, J. Eng. Math. 64 (2009) 281–301.
[5] R. Bustamante, Transversely isotropic nonlinear magneto-active elastomers, Acta Mech. 210 (2010) 183–214.
[6] I.A. Brigadnov, A. Dorfmann, Mathematical Modeling of Magneto- Sensitive Elastomers, Int. J. Solids Struct. 40 (2003) 4659–4674.
[7] A. Dorfmann, R.W. Ogden, Magnetoelastic modelling of elastomers, Eur. J. Mech. A/Solids 22 (2003) 497–507.
[8] A. Dorfmann, R.W. Ogden, Nonlinear magnetoelastic deformations, Q. J. Mech. Appl. Math. 57 (2004) 599–622.
[10] M.R. Jolly, J.D. Carlson, B.C. Muñoz, A model of the behaviour of magnetorheological materials, Smart Mater. Struct. 5 (1996) 607–614.
[11] M. Otténio, M. Destrade, R.W. Ogden, Incremental magnetoelastic deformations, with application to surface instability, J. Elast. 90 (2008) 19–42.
[12] Z. Varga, G. Filipcsei, M. Zrínyi, Magnetic field sensitive functional elastomers with tuneable elastic modulus, Polymer 47 (2006) 227–233.
[13] K. Danas, S.A. Kankanala, N. Triantafyllidis, Experiments and modelling of iron-particle-filled magnetorheological elastomers, J. Mech. Phys. Solids 60 (2012) 120–138.
[14] J. Kaleta, M. Krolewicz, D. Lewandowski, Magnetomechanical properties of anisotropic and isotropic magnetorheological composites with thermoplastic elastomer matrices, Smart Mater. Struct. 20 (2011) 1–12.
[15] T. Borbath, S. Guenther, D.Y. Borin, T. Gundermann, S. Odenbach, X$\mu$CT analysis of magnetic field-induced phase transitions in magnetorheological elastomers, Smart Mater. Struct. 21 (2012) 1–7.
[16] G. Zhou, Shear properties of a magnetorheological elastomer, Smart Mater. Struct. 12 (2003) 139–146.
[17] L. Chen, X.L. Gong, W.Q. Jiang, J.J. Yao, H.X. Deng, W.H. Li, Investigation on magnetorheological elastomers based on natural rubbers, J. Mater. Sci. 42 (2007) 5483–5499.
[18] L. Chen, X.L. Gong, W.H. Li, Microstructures and viscoelastic properties of anisotropic magnetorheological elastomers, Smart Mater. Struct. 16 (2007) 2645–2650.
[20] Y. Xu, X. Gonbg, S. Xuan, W. Zhang, Y. Fan, A high-performance magnetorheological material: preparation, characterization and magnetic-mechanic coupling properties, Rheol. Acta 49 (2011) 733–740.
[21] M. Hossain, G. Possart, P. Steinmann, A small-strain model to simulate the curing of thermosets, Comput. Mech. 43 (2009) 769–779.
[22] M. Hossain, G. Possart, P. Steinmann, A finite strain framework for the simulation of polymer curing, Part I: Elast. Comput. Mech. 44 (5) (2009) 621–630.
[23] M. Hossain, G. Possart, P. Steinmann, A finite strain framework for the simulation of polymer curing. Part II: viscoelasticity and shrinkage, Comput. Mech. 46 (3) (2010) 363–375.
[24] M. Hossain, P. Steinmann, Modelling and simulation of the curing process of polymers by a modified formulation of the Arruda–Boyce model, Arch. Mech. 63 (5–6) (2011) 621–633.
[25] P. Steinmann, M. Hossain, G. Possart, Hyperelastic models for rubber-like materials: consistent tangent operators and suitability for Treloar's data, Arch. Appl. Mech. 82 (9) (2012) 1183–1217.
[26] M. Hossain, P. Steinmann, More hyperelastic models for rubber-like materials: consistent tangent operators and comparative study, J. Mech. Behav. Mater. 22 (1–2) (2013) 27–50.
[27] C. Liebl, M. Johlitz, B. Yagimli, A. Lion, Three-dimensional chemo-thermo-mechnically coupled simulation of curing adhesives including viscoplasticity and chemical shrinkage, Comput. Mech. 49 (5) (2012) 603–615.
[28] C. Liebl, M. Johlitz, B. Yagimli, A. Lion, Simulation of curing-induced viscoplastic deformation: a new approach considering chemo-thermomechanical coupling, Arch. Appl. Mech. 82(8), 2012, 1133–1144.
[29] A. Lion, P. Höfer, On the phenomenological representation of curing phenomena in continuum mechanics, Arch. Mech. 59 (2007) 59–89.
[30] A. Lion, M. Johlitz, On the representation of chemical ageing of rubber in continuum mechanics, Int. J. Solids Struct. 49 (10) (2012) 1227–1240.
[31] M. Johlitz, On the representation of ageing phenomena, J. Adhes. 88 (7) (2013) 620–648.
[32] B. Yagimli, A. Lion, Experimental investigations and material modelling of curing processes under small deformations, Z. Ang. Math. Mech. 91 (2011) 342–359.
[33] M. Kiasat, Curing shrinkage and residual stresses in viscoelastic thermosetting resins and composites (Ph.D. thesis), TU Delft, The Netherlands, 2000.
[34] S. Klinge, A. Bartels, P. Steinmann, Modeling of curing processes based on a multi-field potential: single and multi-scale aspects, Int. J. Solids Struct. 49 (2012) 2320–2333.
[35] K.T. Gillen, Effect of cross-links which occur during continuous chemical stress-relaxation, Macromolecules 21 (1988) 442–446.
[36] J. Lubliner, A model of rubber viscoelasticity, Mech. Res. Commun. 12 (1985) 93–99.
[37] S. Reese, S. Govindjee, A theory of finite viscoelasticity and numerical aspects, Int. J. Solids Struct. 35 (1998) 3455–3482.
[38] P. Saxena, M. Hossain, P. Steinmann, A theory of finite deformation magneto-viscoelasticity, Int. J. Solids Struct. 50 (24) (2013) 3886–3897.
[39] P. Saxena, D.K. Vu, P. Steinmann, On rate-dependent dissipation effects in electro-elasticity, Int. J. Non-Linear Mech. 62 (2014) 1–11.
[40] P. Saxena, M. Hossain, P. Steinmann, Nonlinear magneto-viscoelasticity of transversally isotropic magneto-active polymers, Proc. R. Soc. A 470 (2014) 20140082.
[41] A.J.M. Spencer, Theory of invariants, in: A.C. Eringen (Ed.), Continuum Physics, vol. 1, Academic, New York, 1971, pp. 239–353.
[42] P. Steinmann, Computational nonlinear electro-elasticity – getting started, in: R.W. Ogden, D.J. Steigmann (Eds.), Mechanics and Electrodynamics of Magneto- and Electro-Elastic Materials, Lecture Notes, CISM Summer School, International Centre for Mechanical Sciences, vol. 527, 2011, Springer-verlag, Vienna, 2009, pp. 181–230.
[43] M. Hossain, P. Saxena, P. Steinmann, Modelling the mechanical aspects of the curing process of magneto-sensitive elastomeric materials, Int. J. Solids Struct. 58 (2015) 257–269.